R. & M. No. 3624

R. & M. No. 3624

MINISTRY OF TECHNOLOGY

AERONAUTICAL RESEARCH COUNCIL
REPORTS AND MEMORANDA

Rectangular and Caret Sails in Supersonic Flow

By L. H. TOWNEND
Aerodynamics Dept., R.A.E., Farnborough

LONDON: HER MAJESTY'S STATIONERY OFFICE
1970
PRICE £1 8*s* 0*d* [£1·40] NET

Rectangular and Caret Sails in Supersonic Flow

By L. H. TOWNEND

Aerodynamics Dept., R.A.E., Farnborough

Reports and Memoranda No. 3624*
January, 1967

Summary.

For free-stream Mach numbers between 10 and 4, a study is made of the profiles assumed and isentropic waves produced in non-viscous flows by two-dimensional sails, under pure tension and of finite weight. At the higher free-stream Mach numbers, large parts of the compression flow are virtually centred, and even for long sails (e.g. 100 ft chord) at a high Mach number (e.g. 10) and low stress (e.g. 5 tons/in^2), the weight of such a membrane need not exceed 1 lb/ft^2. The analysis is modified to include the effects of skin friction and is then extended to singly-curved 'caret' sails, which allow leading edges to be swept but can still produce two-dimensional waves; while their curvature imparts to such sails a stiffness-due-to-shape, it is shown that equilibrium can alternatively be maintained by appropriately applied tensile forces. Rectangular and/or caret sails may find applications as wings, intakes, cowls and nozzles for hypersonic vehicles.

LIST OF CONTENTS

*Replaces R.A.E. Tech. Report No. 67006—A.R.C. 29 541.

---

1. *Introduction.*

The use of flexible membranes for producing lift and/or drag forces from incompressible flows[1,2] has long been regarded as standard technique (e.g. for sailing ships and parachutes). More recently, supersonic parachutes for the deceleration of re-entry bodies have been studied in various forms[3,4,5], and since 1960, much American work has been reported on the theoretical and experimental performance of the supersonic parawing[6-14]; this is a type of lifting device comprising a flexible membrane tethered between two stiff leading edge members so as to form (for example as in Fig. 1a) a conically-curved delta wing. Such devices offer the possibility of partial or full retraction or deployment during the flight or re-entry of a parent body.

The flow around such wings is of course rather complex; no attempt appears to have yet been made to simplify their aerodynamics by using a cylindrically curved 'waverider' parawing to 'contain' a two-dimensional flow[15,16] behind a plane shock wave or waves, as in Fig. 1b and 1c. However in 1958, Daskin and Feldman[17] examined the aerodynamic properties and geometric form of a constant chord sail, which they assumed to produce a two-dimensional influence on a hypersonic flow, as in Fig. 1d. In their analysis, which was based on a modified Newtonian approximation[18], they assumed that the sail was of negligible weight and stiffness, that tension was constant across the chord (i.e. that skin friction was also negligible) and that pressure increments due to sail porosity and boundary-layer growth (or separation) were negligible. Daskin and Feldman also stated that they had studied the weight of sails of low and high aspect ratio and of delta planform, that of these the weight was largely due to the 'spars' to which the membrane was attached, but that when compared with conventional wings of identical materials, stress levels and planform, reductions in total weight of 80 to 90 per cent were observed. In 1959, Fink[19] produced a linearised analysis of the impermeable sail in supersonic flow, and in 1960, Boyd[20] extended the analysis of Daskin and Feldman by the inclusion of Busemann's centrifugal correction to Newtonian flow; in a second paper[21], Boyd re-analysed the supersonic sail by means of simple wave theory according to Busemann's Second Order approximation and in 1962 and 1963, investigated[22,23] the effects of porosity. All analyses have indicated that sail profiles would have a progressive increase in camber towards the trailing edge, but as far as is known, no tests on the aerodynamics of two-dimensional sails have been reported, though tests on rigid, concave, wedges in supersonic flow have been reported by Johannesen[24], Connors, Woollett and Blue[25], Chapman[26,27], Larson[26,27] and Kuehn[26-28], Sterrett and Emery[29], and unpublished work briefly mentioned by Ferri[30]: however, all these tests were primarily aimed at investigation of compressible boundary layers in adverse pressure gradients, or of the achievement of centred compression.

In this Report, analyses are presented for two-dimensional sails producing isentropic effects on super- and hypersonic flows of zero or finite viscosity; the assumptions made are that membrane weight and upper surface pressure are both finite, but that, as in other analyses[17,19-21], stiffness and pressure increments due to porosity and boundary-layer growth (or separation) are negligible. Over a wide range of

inflow Mach numbers and for extents of isentropic compression which would be useful for wings or intakes, it is found that two-dimensional sails in non-viscous flow can produce very nearly centred compression (i.e. reversed Prandtl-Meyer waves); furthermore, even for long sails (e.g. 100 ft chord) at high Mach number (e.g. 10) and low stress (5 tons/in^2), the weight per unit wetted area of a steel membrane need not exceed 1 lb/ft^2. In addition, a form of sail is proposed by which two-dimensional isentropic compression would, in principle, be produced and contained at design conditions, but to which single (but not necessarily conical) curvature imparts a stiffness-due-to-shape: it is then shown that exploitation of this stiffness can be reduced (to zero if required) by application to the sail of appropriate tensile forces. Suggestions are made for the application of sail techniques in the design of wings, intakes, cowls and nozzles for hypersonic vehicles.

The analysis does not include any consideration of membrane stability (either static or dynamic), and does not cover low-speed or transonic flight speeds. Flutter, divergence, creep and material degradation at high temperatures are recognised as possible problems, but are not considered in the present analysis.

2. *Properties of Rectangular Sails in Newtonian Flow.*

Daskin and Feldman[17], Fink[19] and Boyd[20,21] have shown that a rectangular membrane tethered along its leading and trailing edges and held at incidence to a uniform free-stream can 'fill', and so form a two-dimensional sail which, with no intermediate constraints and at constant tension, is maintained in a particular profile by the pressure field so generated. The four analyses are based respectively on Newtonian[17], linearised[19], Busemann-Newtonian[20] and Busemann Second Order[21] theories, and as a consequence, predict differing profiles:

(i) Daskin and Feldman[17] (upper surface pressure assumed $p_u = p_\infty \cdot \cos^2\theta$):

$$\frac{p_{\text{ref.}}\, x}{T} = \operatorname{cosec}\Theta - \operatorname{cosec}\theta\,, \frac{p_{\text{ref.}}\, y}{T} = \log_e\left[\tan\frac{\theta}{2}\cdot\cot\frac{\Theta}{2}\right]$$

(ii) Boyd[20] (upper surface pressure assumed to be zero):

$$\frac{p_{\text{ref.}}\, x}{T} = \tfrac{1}{2}(\operatorname{cosec}\Theta - \operatorname{cosec}^2\theta\,.\sin\Theta)\,, \frac{p_{\text{ref.}}\, y}{T} = \cos\Theta - \cot\theta\,.\sin\Theta$$

(iii) Fink[19]:

$$\frac{4q_\infty}{\sqrt{M_\infty^2-1}}\,\frac{x}{T} = \cos\theta - \cos\Theta + \log_e\left[\tan\frac{\theta}{2}\cdot\cot\frac{\Theta}{2}\right], \frac{4q_\infty}{\sqrt{M_\infty^2-1}}\,\frac{y}{T} = \sin\theta - \sin\Theta$$

(iv) Boyd[21]:

$$\frac{4q_\infty}{\sqrt{M_\infty^2-1}}\,\frac{x}{T} = \int_\Theta^\theta \frac{\cos\theta\,.\,d\theta}{\theta}\,, \frac{4q_\infty}{\sqrt{M_\infty^2-1}}\,\frac{y}{T} = \int_\Theta^\theta \frac{\sin\theta\,.\,d\theta}{\theta}\,.$$

In these expressions,

$p_{\text{ref.}}$ = stagnation pressure behind a normal shock,

x, y = orthogonal co-ordinates as in Fig. 2a,

T = tension per foot span of sail,

Θ = sail angle at leading edge,

θ = sail angle at any other point,

and

$$q_\infty = \tfrac{1}{2}\rho_\infty V_\infty^2 \left[= \gamma p_{\text{ref}}/(\gamma+1)^{\frac{\gamma}{\gamma-1}} \left(\frac{(\gamma+1)M_\infty^2}{2(2\gamma M_\infty^2-(\gamma-1))} \right)^{\frac{1}{\gamma-1}} \right].$$

Note that although Boyd's Newtonian analysis[20] was for the model of Fig. 2a, his results apply with equal validity to that of Fig. 2b in which the inclusion of a wedge is thought to be realistic, both from considerations of leading-edge heating and sail tethering. Fig. 2c shows typical sail shapes and it is seen that

(1) they are somewhat similar to streamlines in a Prandtl-Meyer corner flow, i.e. a centred expansion or compression wave, but that

(2) $\Theta = 0$ is impossible except for infinite tension, so that some flow deflection and loss of stagnation pressure through a leading-edge shock wave must occur for any structurally realistic sail.

The first feature encourages investigation of sails which produce isentropic compression, since such sails might offer simultaneously, a useful type of flow and a low membrane weight; the second feature suggests that, at least for sails producing purely isentropic compression, a new analysis is needed rather than an attempt to extend Boyd's work. An analysis of the isentropic flow beneath a (supersonic or hypersonic) two-dimensional sail, and its relation to that through a centred wave, is described in the next Section.

3. *Properties of Rectangular Sails in Isentropic Flow.*

3.1. *Sails Producing Centred Waves.*

Consider first a weightless, infinitely flexible, non-porous membrane in conditions of zero flow and supporting at constant tension a pressure difference, distributed along its length in such a way that the profile it assumes is identical with a streamline in a centred (i.e. a Prandtl-Meyer) wave; that is let the membrane profile be

$$\frac{r}{r_0} = \frac{1}{\cos^{1/k^2} k\phi} \quad (\textit{see} \text{ Appendix A and Fig. 3}). \tag{1}$$

It can then be shown (again *see* Appendix A) that the required distribution of pressure difference (P.D.) is

$$\frac{(P.D.)\,r_0}{T} = \frac{(p_l - p_u)\,r_0}{T} = \left(\frac{1}{k^2}-1\right) \frac{\tan^2 k\phi \,.\, \cos^{1/k^2} k\phi}{\left(1+\frac{1}{k^2}\tan^2 k\phi\right)^{3/2}}$$

in which

$$k^2 \equiv \frac{\gamma-1}{\gamma+1}\left(= \frac{1}{6} \text{ if } \gamma = 1{\cdot}4 \right). \tag{2}$$

Suppose now that this same membrane is tethered in a supersonic stream and that the lower surface pressure p_l is generated by a Prandtl-Meyer wave so that, at any point,

$$\frac{p_l}{p_T} = \left(1+\frac{\gamma-1}{2}M^2\right)^{-\frac{\gamma}{\gamma-1}} = 1\Big/\left(1-\frac{k^2}{k^2-1}\left[1+\frac{1}{k^2}\tan^2 k\phi\right]\right)^{\frac{k^2+1}{2k^2}} \equiv F(k\phi)\,;$$

then the distribution of pressure on the upper surface required to ensure that the membrane retains its shape (and so that equations (1) and (2) retain their validity), is

$$\frac{p_u r_0}{T} = \frac{p_l r_0}{T} - \left(\frac{1}{k^2} - 1\right) \frac{\tan^2 k\phi \,.\, \cos^{1/k^2} k\phi}{\left(1 + \frac{1}{k^2}\tan^2 k\phi\right)^{3/2}} = \frac{p_l r_0}{T} - \left(\frac{1}{k^2} - 1\right) f(k\phi)$$

i.e.

$$\frac{p_u}{p_T} = \frac{1}{\left(1 - \frac{k^2}{k^2-1}\left[1 + \frac{1}{k^2}\tan^2 k\phi\right]\right)^{\frac{k^2+1}{2k^2}}} - \left(\frac{1}{k^2} - 1\right)\frac{f(k\phi)}{p_T r_0/T}$$

$$= F(k\phi) - \left(\frac{1}{k^2} - 1\right)\frac{f(k\phi)}{p_T r_0/T}. \tag{3}$$

In Fig. 3 the variation with $k\phi$ of the airflow function $F(k\phi)$ is shown and, for various values of $p_T r_0/T$, that of the membrane function $\left(\frac{1}{k^2} - 1\right)\frac{f(k\phi)}{p_T r_0/T}$. It is seen that, for $k\phi < 25°$ (approximately) i.e. for $M < 1{\cdot}5$ (approximately), the slope of the latter precludes any close alignment with $F(k\phi)$; however for $p_T r_0/T = 1/1{\cdot}40$ and $1/1{\cdot}51$, the curve for the membrane function crosses that of the airflow function at Mach numbers of about 3 and 7 respectively, the former being nearly coincident with $F(k\phi)$ at $30° \leqslant k\phi \leqslant 70°$ (that is, at lower surface Mach numbers between about 1·75 and 7). But the vertical distance by which, at a given $k\phi$ and $p_T r_0/T$, the airflow function lies above the membrane function is equal to p_u/p_T in equation (3) and its variation with $k\phi$ thus represents the distribution of upper surface pressure which is required for a sail at the chosen value of $p_T r_0/T$ to produce a centred compression; thus in the range of values of $k\phi$ for which airflow and membrane curves are nearly coincident, a sail having zero upper-surface pressure might be expected to give 'nearly centred' compression. If $p_T r_0/T$ is increased slightly, a nearly centred compression might be expected from a sail having a low, constant value for upper-surface pressure. For the weightless sail giving precisely centred compression, the necessary distribution of upper-surface pressure is shown in Fig. 4 as the variation of $\left[F(k\phi) - \left(\frac{1}{k^2} - 1\right)\frac{f(k\phi)}{p_T r_0/T}\right]$ with $k\phi$ (i.e. with local Mach number). As is predictable from Fig. 3, rather rapid changes in the function are required at $M < 1{\cdot}5$. For higher values of Mach number, acceptable (i.e. positive) values of $\left[F(k\phi) - \left(\frac{1}{k^2} - 1\right)\frac{f(k\phi)}{p_T r_0/T}\right]$ lie between the $k\phi$−axis and the asymptote $(p_T r_0/T) = \infty$, for which condition

$$F(k\phi) - \left(\frac{1}{k^2} - 1\right)\frac{f(k\phi)}{p_T r_0/T} = F(k\phi) = \left(1 + \frac{\gamma - 1}{2} M^2\right)^{-\frac{\gamma}{\gamma - 1}};$$

as shown from the values tabulated in Fig. 4, the variation of $F(k\phi)$ at high values of $k\phi$ (or M) is not rapid.

It is emphasised that both Figs. 3 and 4 merely show values which are required to satisfy equation (3), but that such values may be unrealistic in the engineering sense; however they encourage the view that sails with constant pressure on the upper surface may produce at least some regions of nearly centred compression. This view is supported by an alternative analysis due to Pike[31], who has compared the radius of curvature of a Prandtl-Meyer streamline with that of a sail having constant tension, zero weight and zero upper-surface pressure; Pike has found that for $\gamma = 1{\cdot}4$ and $M > 7$, these radii differ by less than 3 per cent, and that as $M \to \infty$, their difference tends to zero.

However neither Pike's analysis nor that above have made due allowance for the effects of independently chosen values of upper-surface pressure and/or sail weight. Further, although it is possible to predict the pressure distribution required to give centred compression, it may be impracticable or inconvenient to provide means for precisely controlling this distribution and in fact, a full-scale requirement might be for the sail to be simply tethered at its leading and trailing edges. Furthermore, the combinations of $p_T r_0/T$ and M indicated in, for example Fig. 4, need provide no more than mathematical validity to the claim that a sail produces a centred wave; it has yet to be shown that such combinations allow structurally feasible sails. Three further steps in the analysis are thus required:

(1) equations for the profile of two-dimensional sails (with finite weight and upper-surface pressure) must be quoted in general form,

(2) the waves produced for various combinations of M_∞ and parameters describing sail tension, chord, pressures and weight must be compared with corresponding Prandtl-Meyer waves, and

(3) values of M_∞ and the other parameters which, in combination, appear to offer engineering feasibility (both aerodynamic and structural) must be identified.

These three steps are now described.

3.2. *Sails Producing Non-Centred Waves.*

In the first part of Appendix B the sail of Fig. 5 is investigated subject to assumptions that tensions due to skin friction, increments in pressure due to sail porosity and/or boundary-layer growth or separation, and effects on shape due to sail stiffness are negligible, and that the change in air temperature through the wave produces negligible change in the value of γ[†].

For a sail in frictionless flow, whose weight is negligible only in comparison with the tension, it is shown in the first part of Appendix B that

$$T\frac{d\theta}{ds} = p_l - (p_u + w\cos(\theta+\theta_c)), \tag{4}$$

and hence that the sail profile is given by

$$\frac{p_{T1}\,x}{T} = \int_{\beta_1}^{\beta} \frac{A}{B}.\cos\theta\,.\,d\beta\,,\quad \frac{p_{T1}\,y}{T} = \int_{\beta_1}^{\beta} \frac{A}{B}.\sin\theta\,.\,d\beta \tag{5}$$

in which

$$A \equiv \left(\frac{1}{1+\beta^2} - \frac{1}{1+k^2\beta^2}\right),\ \beta^2 = M^2 - 1\,,$$

$$B \equiv \left[\left(1+\frac{\gamma-1}{2}M^2\right)^{-\frac{\gamma}{\gamma-1}} - \frac{p_u + w\cos(\theta+\theta_c)}{p_{T1}}\right].$$

Note that $p_{T1}\,x/T$ (and $p_{T1}\,y/T$) must be positive numbers since in each, all three constituents are positive. Also in the integrals (5), $M_1 > M$ so that $\beta_1 > \beta$; thus, for positive values of θ to give positive values for $p_{T1}\,x/T$ and $p_{T1}\,y/T$, it is required that A/B should be negative. But if $\gamma > 1$, then $0 < k^2 < 1$, and since β^2 is positive, A is always negative; thus B must always be positive, that is,

---

[†]These assumptions apply to all sails considered in the main text of this Report, although in the analyses presented in the second part of Appendix B and in Appendix C, the effects of skin friction on the equilibrium of rectangular and 'caret' sails are noted.

$$\left(\frac{1}{1+\frac{\gamma-1}{2}M^2}\right)^{\frac{\gamma}{\gamma-1}} - \frac{p_u + w\cos(\theta_c+\Theta)}{p_{T1}} \geqslant 0 \text{ in which} \left(1+\frac{\gamma-1}{2}M^2\right)^{\frac{\gamma}{\gamma-1}} = \frac{p_T}{p} = \frac{p_{T1}}{p}$$

i.e.

$$\frac{p_u}{p_\infty} + \frac{w}{p_\infty}\cos(\theta_c+\Theta) \leqslant \frac{p}{p_\infty}.$$

At the leading edge of a sail producing fully isentropic compression,

$$M_N = 1, \frac{p_1}{p_\infty} = \frac{2\gamma M_N^2 - (\gamma-1)}{\gamma+1}\Bigg]_{M_N=1} = 1 \text{ and } \Theta = 0$$

i.e.

$$\left(\frac{p_u}{p_\infty} + \frac{w}{p_\infty}\cos\theta_c\right)_{M_N=1} \leqslant 1 ;$$

but unless some disturbances occur in the flow over the top of the leading edge, then at this leading edge, $p_u/p_\infty = 1$ and the above condition is satisfied only for negative values of w/p_∞ (i.e. for sails of negative weight) or for $w/p_\infty = 0$. If $w/p_\infty = 0$ and $p_u/p_\infty = 1$ then the sail is of zero curvature and so produces no influence, isentropic or otherwise, upon the stream. It follows that, if $p_u/p_\gamma = 1$, it is impossible to start an isentropic compression by a sail in pure tension. Of course, if the forepart is stiffened and of isentropic profile, the remainder can be tensioned as a sail. Alternatively, a sail may be attached to a plane wedge, as in Fig. 5, so that p_u/p_∞ may be less than unity; if $w/p_\infty = 0 = p_u/p_\infty$ then conditions correspond, as nearly as is possible for an isentropic sail, to those assumed by Boyd[20]. In Fig. 6a, for $p_u/p_\infty = 0$, $M_N = 1$ and $w/p_\infty = 0, 0{\cdot}2$ and $0{\cdot}4$, sail profiles are drawn for free-stream and discharge Mach numbers (M_∞ and M_{comp}) of 10 and 3·5 respectively; sail profiles are shown in the top two sketches, firstly as computed (*see* Acknowledgment) in terms of $p_{T1}\,x/T$ and $p_{T1}\,y/T$, and secondly, for direct comparison at equal chord. Sketch A shows, as did Daskin and Feldman[17], Fink[19] and Boyd [20,21] for the weightless sail, that curvature increases rapidly towards the trailing edge and also that, as sail weight rises, then for a given extent of compression $p_{T1}\,x/T$ also rises, so that, for given values of p_{T1} and sail chord, tension is consequently reduced; Sketch B shows that, the heavier the sail, the more rapid is the rate of increase of curvature towards the trailing edge, with the result that, since regions of small dy/dx extend over larger proportions of the chord, the heavier but more moderately tensioned sails lie above the lighter sails. From this fact it also follows that for the heavier sails, the first characteristic of the sail flow (i.e. that at which streamline curvature is initiated) lies further from the trailing edge; but in the three drawings showing wave positions (for $p_u/p_\infty = 0$ and $w/p_\infty = 0, 0{\cdot}2$ and $0{\cdot}4$, and for sail chords of approximately 100 inches), it is further seen that compression waves corresponding to local Mach numbers between 7 and 3·5 are nearly centred*. In Fig. 6b, the effect of changing the upper surface pressure to $p_u/p_\infty = 0{\cdot}5$ is seen to be a significant change in the positions of initial waves, but little change in the centring of later waves. Finally Fig. 6c shows, for two values of p_u/p_∞, the lifting effectiveness (C_L) and efficiency (L/D) of sails in non-viscous flow at $M_\infty = 10$, and also at $M_\infty = 7$ and 4. The wedge-spar is assumed to be extremely thin, so that the forces and flow losses it produces may be neglected; the lift coefficient may then be written as

$$C_L = T\sin(v_\infty - v_{\text{comp}})/q_\infty\, x = \sin(v_\infty - v_{\text{comp}}) \Big/ \left(\frac{q_\infty}{p_{T_\infty}} \cdot \frac{p_{T_\infty}}{p_{T1}} \cdot \frac{p_{T1}\,x}{T}\right),$$

*In practice, convergent characteristics would coalesce into a shock wave, together with a reflected wave which would be either an expansion or a compression, according to the value of M_γ and the extent of compression due to the sail; for clarity in Figs. 6–9, such interactions are not shown.

and L/D and turning angle as

$$\left.\frac{L}{D}\right]_{\text{non-viscous}} = \left.\frac{L}{D}\right]_{\text{const. } T} = \frac{T \cdot \sin(\nu_\infty - \nu_{\text{comp}})}{T(1-\cos(\nu_\infty - \nu_{\text{comp}}))} = \cot\frac{\nu_\infty - \nu_{\text{comp}}}{2}.$$

Due to the assumptions that γ is constant and that the flow is isentropic (i.e. $p_{T1} = p_{T_\infty}$), local values of static pressure ratio are given as

$$\frac{p}{p_\infty} = \frac{p}{p_{T1}} \cdot \frac{p_{T_\infty}}{p_\infty} = \left(\frac{2+(\gamma-1)M_\infty^2}{2+(\gamma-1)M^2}\right)^{\frac{\gamma}{\gamma-1}};$$

thus lines of constant static pressure ratio may be added to Fig. 6c to show the pressure rise the boundary layer is required to sustain. For sails yielding a high value of L/D at $M_\infty = 10$, these may not be too severe (in view of the figure quoted by Ferri[30], namely a static pressure ratio of 175 without separation of a laminar boundary layer); however, the lifting performance of isentropic sails is rather poor in comparison with that of the simple wedge (e.g. the plane shock Nonweiler wing) for which values of C_L and L/D are as shown below

Flow deflection (degrees)	$\frac{L}{D}_{\text{non-viscous}}$	C_L for $p_u/p_\infty = 0$ and			C_L for $p_u/p_\infty = 0{\cdot}5$ and			C_L for $p_u/p_\infty = 1$ and		
		$M_\infty = 10$	7	4	$M_\infty = 10$	7	4	$M_\infty = 10$	7	4
6·340	9	0·055	0·079	0·162	0·048	0·064	0·118	0·041	0·050	0·074
8·130	7	0·075	0·100	0·189	0·068	0·085	0·145	0·061	0·071	0·101
11·310	5	0·119	0·146	0·244	0·112	0·132	0·200	0·105	0·118	0·157
18·435	3	0·258	0·287	0·398	0·251	0·274	0·356	0·245	0·260	0·314

It follows that, in purely lifting applications, isentropic sails may be less desirable than conventional bodies unless they allow great improvements in structure weight, or other features such as greater lengths of laminar flow. Alternatively a sail may be used as part of a body beneath which a shock wave forms; for these, values of C_L and L/D would have to be recalculated. If at $M_\infty = 10$, a sail is mounted behind a wedge-spar producing a shock-wave ($M_N = 1{\cdot}4$ in Figs. 7a and 7b), the effects of variations in w/p_∞ on sail profile and its position relative to the first characteristic of the sail flow (*see* Sketch B) are much reduced, and nearly centred compression is obtained over a similar range of local Mach number; in Figs. 7c and d, only weightless sails are shown since with $M_N = 2{\cdot}6$, the effects of w/p_∞ on profile are extremely small.

As seen from Figs. 6–7, $p_{T1}\, x/T$ always increases with w/p_∞ if the values of other parameters are held constant. In Fig. 8 and 9 ($M_\infty = 7$ and 4 respectively) plots of $p_{T1}\, x/T$ are not shown since (as can be seen from Table 1) this trend with w/p_∞ is unchanged.

In Figs. 8a and 8b, the effects of w/p_∞ on sails at $M_\infty = 7$ and $M_N = 1{\cdot}2$ are seen to be significant, but even for $w/p_\infty = 0$, early compression waves lie well below the near-focus of waves in the range $5 \geqslant M \geqslant 2{\cdot}5$. If M_N is increased to 2 (*see* Figs. 8c and d) the effects of variations in w/p_∞ are slight and

for both values of p_u/p_∞, much of the compression flow is nearly centred. For sails operating at $M_\infty = 4$ and $M_N = 1{\cdot}2$ (*see* Figs. 9a and b) the influence of w/p_∞ is considerable but even at $w/p_\infty = 0$ and for the rather short sails drawn, early waves lie well below the points at which later waves intersect, and no part of the compression flow can be described as centred; if $M_N = 1{\cdot}6$ as in Figs. 9c and d, the influence of w/p_∞ is reduced but again, even for weightless sails, early waves lie below the intersections of later waves, and even the latter are not closely centred.

It is tentatively concluded from Figs. 6 to 9 that:

(1) in non-viscous hypersonic flows it is possible to produce significant extents of nearly centred compression beneath sails in pure tension,

(2) as free-stream Mach number falls to supersonic values, centring of the waves becomes less marked,

(3) at a given free-stream Mach number, increases in upper-surface pressure and/or sail weight usually increase the gaps between initial compression waves and the near-focus of later waves,

(4) at a given free-stream Mach number, an increase in the wedge-spar angle reduces the influence of upper-surface pressure and of sail weight.

It has been shown in Figs. 6 to 9 and Table 1 that a choice of M_∞, M_N, w/p_∞ and p_u/p_∞ leads as a mathematical requirement to a particular value of $p_{T1}\,x/T$; the final paragraphs of this section relate to the engineering acceptability of these combinations of M_∞, M_N, $p_{T1}\,x/T$ and w/p_∞.

For a sail tethered to the trailing edge of a wedge-spar as in Fig. 5,

$$\frac{p_{T1}\,x}{T} \equiv \frac{p_{T1}}{p_{T_\infty}} \cdot \frac{p_{T_\infty}}{p_\infty} \cdot \frac{p_\infty\,x}{T} \equiv \left[\frac{2+(\gamma-1)\,M_\infty^2}{2+(1-\eta_{KE})\,(\gamma-1)\,M_\infty^2}\right]^{\frac{\gamma}{\gamma-1}} \frac{p_\infty\,x}{T} \tag{6}$$

in which, for a given value of M_∞, (1) η_{KE} prescribes the strength of the shock on the wedge-spar and hence M_N and M_1, (2) p_∞ implies an equivalent air speed (E.A.S.) at which the sail is operating and (3) x is the sail chord. If these parameters are allotted numerical values, then for a chosen value of $p_{T1}\,x/T$, a particular value will result for T, the sail tension per foot span. For example, in Fig. 10 the variation with T of $p_{T1}\,x/T$ is shown for sails having $x = 1$, 10 and 100 ft, and operating at different values of M_∞ (10, 7 and 4) and at such altitudes as give identical values of E.A.S. (350 knots); in each case the effects of varying shock strength are indicated by η_{KE} values of 1·0 and 0·99, which represent shock strengths from zero to those which would be adequate for initiating intake processes. Extra scales have been added to indicate (1) the thickness of sails which would operate at specified tensile stresses (5 tons/in^2 and 10 tons/in^2), and (2) the sail weight per unit wetted area which would result for a sail material such as high quality stainless steel (which has a density of 0·28 lb/in^3). Note that, even for the lower stress level (5 tons/in^2), sail thickness and weight need not exceed values of 0·05 inch (approximately 18 S.W.G.) and 2 lb/ft^2 respectively; the corresponding value of sail tension (i.e. of spar loading) is about 7000 lb/ft span.

It is seen that the values of $p_{T1}\,x/T$ for aerodynamically and structurally realistic operating conditions lie between 10 and 10 000; thus the values of $p_{T1}\,x/T$ required in Figs. 6 to 9 (lying in the 'boxes' on Fig. 10 and listed in Table 1) can be compatible with engineering realism, and for 350 knots E.A.S., $w/p_\infty = 0{\cdot}4$ would frequently be an excessively high estimate of sail weight, even for stress levels as low as 5 tons/in^2.

Fig. 10 is in fact restricted to use for an E.A.S. of 350 knots; however, in that figure, tabulated values of E.A.S. and p_∞ show how, at various values of M_∞ variations in the flight environment would occur, and use of these values of p_∞ in equation (6) would allow Fig. 10 to be re-drawn for other values of E.A.S.

It is concluded from Fig. 10 that values of $p_{T1}\,x/T$ selected in Figs. 6 to 9 and Table 1 to give mathematical consistency with the chosen values of p_u/p_∞ and w/p_∞, need not prevent two-dimensional sails from being realistic in the engineering sense. It is therefore worth examining the possible use of sail techniques in three-dimensional (caret) sails having swept leading edges; the geometry, aerodynamics and statics of such sails are now described.

4. *Properties of Caret Sails in Isentropic Flow.*

It is known[32] that, at design conditions of Mach number and incidence, two-dimensional, centred,

isentropic waves can in principle be formed by and contained between so-called 'caret' surfaces, such as those of Fig. 11a; if the leading edges of such surfaces are straight then each surface is of conical curvature through the tip T, and each is developable onto a plane (*see* inset to Fig. 11a). More generally, surfaces of single but non-conical curvature (*see* Fig. 11b) may also produce and contain two-dimensional but non-centred isentropic waves; these may also be individually wrapped from initially flat flexible foils of correct developed planform.

Consider the case in which the foils are of thin metal and have in consequence a small but non-zero stiffness; then, if wrapped to form caret surfaces of conical or merely single curvature, such foils will acquire by curvature an additional stiffness-due-to-shape. For example, consider a triangular plane Foil A mounted on a rigid wall as in Fig. 11c. Application of a load P at the tip will produce deflection until (at the position shown dotted) the foil has stored, under elastic strain, an energy equal to the work done by P. Consider now a similar foil, similarly mounted but conically curved through the tip as is Foil 'B'; unless failure of the mounting, or wrinkling and/or buckling of the foil occurs, the application at the tip of the same force P will now produce a smaller tip deflection, demonstrating that a stiffness-due-to-shape has been acquired even though the foil thickness and material remain unchanged. Further, the foil will be in some measure resistant to a load (or loads) acting in any direction at the tip or elsewhere although the level, nature and effects of the stresses in the foil will depend upon the loading distribution and upon the foil curvature, anhedral, sweep, aspect ratio, material properties and thickness; however for a material such as thin steel sheet the acquired stiffness would frequently be enough to save a caret foil, unlike a two-dimensional foil, from distorting under its own weight. Finally the arguments above will apply not only to a curved foil mounted on a rigid wall, but may be extended to paired foils (C and D in Fig. 11c) in which geometrically compatible foils are connected (e.g. by a seam weld) along the ridge line; for cases in which foil curvature leads to a curved ridge line, the foils become thereby mutually stiffening, although in the absence of a rigid wall, they may suffer some chordwise bending.

For such paired foils, two conclusions should be valid:

(1) for a given operating condition, the structure weight should be favourably influenced by the acquired stiffness, and

(2) since each surface can be wrapped from sheet material, fabrication may be simple.

Clearly, skin wrinkling and flutter characteristics must be investigated for the various types of loading distributions expected. These are likely to be complex[8,12,33]; however, at least the statics of such foils are simple, since as shown below, and as already investigated for the simpler case of the rectangular sail, each element of the membrane can be held in equilibrium under a pressure difference and an appropriate distribution of purely tensile force.

4.1. *The Geometry and Aerodynamics of Caret Sails.*

In Fig. 12a, Flow Model III shows various streamlines along any one of which a flexible surface, of correct chord and suitably tensioned between suitable points, would align itself. Large and small sail elements could, in principle, be assembled to form a 'stepped sail' comprising

(1) individual ribbons, each at a tension appropriate (and in fact for a given value of $p_{T1}\, x/T$ proportional) to its chord, and

(2) appropriately shaped sidewalls, which must resist the sideforces produced by internal pressures.

If a sail of single curvature is formed as in Fig. 12b, this also (having non-zero anhedral) will be subject to sideforces. For a non-centred flow such as Model III, the sail of Fig. 12b is non-conical; however, any two Mach waves between which Mach number changes by an infinitesimal amount, may be regarded as having a focal line (Oy' in Fig. 12b) and will be associated with a conically curved strip $A\,B\,C\,D$ of the singly (but not conically) curved sail $A'\,B'\,C'\,D'$.

Consider the geometry of an element E of this sail. The axis Oy' is the focal line of the compression waves from $A\,D$ and $B\,C$ (i.e. the 'instantaneous focal line' for a part of a non-centred flow); Ox' and Oz' form an orthogonal system of axes with Oy', in which system Ox' is aligned with the inflow direction (given by M_1 or $k\phi_1$), so that Oz' is then at a defined angle to the sonic plane ($M = 1$, $k\phi = 0$) of the given two-dimensional flow. Suppose that the caret sail profile, with which the element E is aligned,

corresponds to streamline S in Fig. 12c: further, for isentropic compression from M_1 to M by a centred (i.e. reversed Prandtl-Meyer) wave, suppose the streamline through element E is S', with whose centre of compression that of S is instantaneously coincident: finally, let streamline S'' be that with which a two-dimensional sail, producing isentropic compression from M_1 to M, would align itself. Since all three waves correspond to isentropic compression from the same initial value of Mach number, their sonic lines are parallel, but not in general collinear. From Figs. 12b and 12c it is clear that an element of length ds and projected width dy', situated at the point at which S, S' and S'' are tangential, will for all these streamlines, form projections onto the plane $x'\,Oy'$, which are of different geometry (rectangular for S' and S'', and trapezoidal for S) but of equal area: similarly the rectangular and trapezoidal projections onto the plane $z'\,Oy'$ will all be of equal area. Since the pressure on the element is identical for all these streamlines, the components of pressure force parallel to Ox' and Oz' are identical; it follows that if any differences arise between the profiles and/or statics of two-dimensional sails and caret sails, these must be due to the third component of pressure force (or to differences in their wetted areas). The third component of pressure force, being parallel to Oy', occurs as a direct result of the caret foil's non-zero anhedral, and so did not enter the two-dimensional analysis of Section 3; its influence on the statics of the caret sail is described below.

4.2. *The Statics of Caret Sails*.*

Of the pressure force on element E, the component P'_z (parallel to Oz') and P'_x (parallel to Ox'), being equal to those on a corresponding element of a two-dimensional sail, will in consequence produce a resultant (P'_{xz} in Fig. 13a) which is identical in magnitude ($= (P.D.)\,ds\,.\,dy$) and direction (parallel to $x'\,Oz'$ and normal to streamline S). The third component P'_y is, by definition, parallel to Oy' and so lies in the same plane as Oy' and the surface generator which passes, as a straight line, through the point O and the centroid of element E. P'_y may thus be replaced by two statically equivalent forces P_r and P_g, of which P_g lies along the generator and is of such a magnitude that P_r lies parallel to $x'\,Oz'$; since P_r passes through the axis Oy' which is the focal line for the flow over element E it follows that the angle between P_r and the streamline S must equal the Mach angle, $\mu\left(=\sin^{-1}\frac{1}{M}\right)$. Thus in the plane which contains the streamline S, both P_r and P'_{xz} can be shown (*see* Fig. 13b); P_r is seen to contribute two components, firstly P'_r which is directly additive to P'_{xz} and is given by

$$P'_r = P_r \sin\mu = P_r/M$$

and secondly

$$P''_r = P_r \cos\mu = P_r\sqrt{(M^2-1)}/M$$

which acts tangentially along the sail chord. Note that

$$P''_r/P'_r = \sqrt{M^2-1}\ \text{i.e.}\ P''_r > P'_r \text{ for } M > \sqrt{2}\,,\ P''_r \doteq M\,P'_r \text{ for } M >> 1\,.$$

It can be further shown (as in Appendix C and Figs. 13c to e) that, for a caret sail in a two-dimensional flow behind a plane shock wave,

$$\frac{P_r}{P'_{xz}} = \frac{K}{M}\left(1+\frac{1}{k^2}(M^2-1)\right)^{1/k^2} = \frac{K}{M}\left(\frac{r}{r_0}\right)^2$$

---

*The author would like to thank Mr. E. G. Broadbent and Dr. C. C. L. Sells for valuable comments on the statics of membranes subject to pressure and tension forces.

in which $K = f(\gamma, M_N, M_\infty, \Lambda)$ i.e. a function of free-stream Mach number, shock wave strength and the true angle of sweep of the wedge-spar leading edge; thus

$$\frac{P'_r}{P'_{xz}} = \frac{K}{M^2}\left(\frac{r}{r_0}\right)^2, \frac{P''_r}{P'_{xz}} = \frac{K}{M^2}\sqrt{M^2-1}\left(\frac{r}{r_0}\right)^2$$

of which both are functions of γ, M_N, M_∞, Λ and the local Mach number, M. Also from Appendix C it is known that for a unit (arc) length of root chord, the net force parallel to a generator required to balance the sum of the P_g-components along the generator of a sail of given span is

$T_{g_{\text{root}}} = \frac{K}{M}\left(\frac{r}{r_0}\right)^2$ (P.D.) sec τ . $(y'_2 - y'_1)$, in which $(y'_2 - y'_1) \equiv$ span of the sail, and $M, \left(\frac{r}{r_0}\right)$, P.D. and τ are constant for the given generator.

Thus, of the three components of pressure force $(P'_{xz} + P'_r)$, P''_r and P_g which act on element E in Fig. 13,

(1) $(P'_{xz} + P'_r)$ can be balanced by tensions acting in a plane parallel to $x'Oz'$,

(2) P''_r can be balanced by a chordwise tension and so contributes to the value of dT/ds, and

(3) P_g can be balanced by a tensile force acting along the local generator (and the sum of the P_g-components along a given generator can be balanced at the root by a single tension, $T_{g_{\text{root}}}$).

These forces are shown in Fig. 13f, from which it is seen that chordwise tension must increase from the leading to the trailing edge; also since the elemental chord of a strip along a surface generator increases linearly from tip to root (the strip being of trapezoidal planform), it follows that the value of $d\theta/ds$ falls linearly and hence that chordwise tension increases linearly from tip to root. Thus the chordwise tension required to act at the inboard end of the trailing edge is a maximum for the whole sail.

It is possible that if the intrinsic stiffness-due-to-shape of the caret sail is to be exploited (other than merely to prevent distortion due to weight, or inertial forces due to acceleration), then some or all of the above forces may be omitted; also if a centred wave is required, necessary modifications to change the profile (from S to S') may be made structurally acceptable by an appropriate choice of some or all of the upper surface pressure distribution, weight distribution, the tensile loading, or the anhedral, thickness or thickness distribution of the foil. To understand the interplay of aerodynamic and structural considerations would require a full stress analysis of aerodynamically acceptable caret sails, and hence the prediction of main flows, base flows and boundary layers on both top and bottom surfaces. Realistic assessment would require better methods of analysis than are available, and also a knowledge of the configuration and conditions in which a sail would be required to operate. This Section therefore closes with a brief study of the effects on sail profile which simultaneous application of the above forces would produce.

If it is assumed that the sum of the P_g-components along a given generator of a caret sail is balanced at the root, then the two remaining forces on each element, P''_r and $(P'_{xz} + P'_r)$, lie in a single plane and calculation of the tensions required to balance them is a problem in two-dimensions only. Appendix B contains two-dimensional analyses for rectangular sails in non-viscous flow ($dT/ds = 0$) and in viscous flow (dT/ds negative); the second of these analyses is extended in Appendix C to include the effects of anhedral on a singly curved caret sail which produces a two-dimensional wave in an isentropic flow. Although this analysis would allow calculation of the tension distribution, sail profile and the form of wave produced, the integral expressions for sail profile have not in fact been programmed in their general form (*see* equations (C.8)); however, the differences to be expected between the profiles assumed in two-dimensional flow by caret and by rectangular sails are indicated below.

For a caret sail the pressure difference which induces chordwise curvature is $(P'_{xz} + P'_r)$ i.e. $P'_{xz}\left(1 + \frac{P'_r}{P'_{xz}}\right)$, the product of the 'two-dimensional pressure difference' P'_{xz}, and the 'anhedral correction factor' $\left(1 + \frac{P'_r}{P'_{xz}}\right)$. The importance of the latter can be found by studying its variation with local Mach number

(M) for typical combinations of γ, M_N, M_∞ and Λ; this variation is shown in Fig. 13g for $M_\infty = 10$, 7 and 4, values of M_N which correspond to $\eta_{KE} = 1{\cdot}0$ and $0{\cdot}99$, and $\Lambda = 50°$, $60°$ or $70°$ according to M_∞. It is seen that the importance of anhedral is greatest at the upstream end of a given sail, that in the worst case ($M_\infty = 4, \eta_{KE} = 0{\cdot}99, \Lambda = 60°$) the value of $\left(1+\frac{P'_r}{P'_{xz}}\right) > 1{\cdot}3$, but that in most cases $\left(1+\frac{P'_r}{P'_{xz}}\right)$ falls rapidly to values $< 1{\cdot}05$. Now for rectangular sails, waves from the upstream end have been seen to lie ahead of the near-focus of later waves; since for a caret sail of zero weight, equation (C.5) simplifies to

$$\frac{d\theta}{ds} = \frac{(p_l - p_u)}{T}\left(1+\frac{P'_r}{P'_{xz}}\right), \tag{7}$$

the existence of relatively high values of $\left(1+\frac{P'_r}{P'_{xz}}\right)$ at the upstream end of a sail will tend to increase the local profile curvature and so at least to reduce the gaps which, beneath rectangular sails, separate early waves from the near-focus of the remainder. However, this statement is valid only if the value of T in equation (7) differs insignificantly from that for the rectangular sail with which comparison is made; but for the latter, T is a constant if weight and skin friction are zero ($dT/ds = 0$), while for caret sails, even of zero weight and in non-viscous flow,

$$\frac{dT}{ds} = (p_l - p_u)\frac{K}{M^2}\left(\frac{r}{r_0}\right)^2 \sqrt{M^2-1} \qquad \text{(See equation (C.4))}$$

Furthermore, tension per unit span of a rectangular sail is constant along the span, whereas for a caret sail its value increases linearly from tip to root, i.e. the chordwise tension on a caret sail reaches a maximum at the inboard end of the trailing edge. However, except for cross-flows in the boundary layers, the flow produced by a caret sail is two-dimensional, so that to study the profile which the sail assumes and the wave it produces, it is sufficient to study only a chordwise strip of very small span (dy' in Fig. 12b say).

Consider such a strip at the root of a singly curved caret sail. The chordwise tension at one point can be chosen to equal that of a given rectangular sail; at this or any other point on the strip, the tension and profile curvature may be related to that of a rectangular sail, by comparing equations (B.3) and (C.5), thus

$$\frac{T}{T_{2.D}} = \frac{\frac{ds}{d\theta}\left[(p_l - p_u)\left(1+\frac{P'_r}{P'_{xz}}\right) - w\cos(\theta+\theta_c)\sqrt{1+\frac{P'_r}{P'_{xz}}}\right]}{\left(\frac{ds}{d\theta}\right)_{2.D}[p_l - (p_u + w\cos(\theta+\theta_c))]}$$

or if $w = 0$,

$$\frac{d\theta/ds}{(d\theta/ds)_{2.D}} = \left(1+\frac{P'_r}{P'_{xz}}\right)\Big/\frac{T}{T_{2.D}}. \tag{8}$$

Suppose that in a comparison between a rectangular sail and a chordwise strip of caret sail, the chordwise tension at one point on the latter is required to equal that of the former i.e. if $T_1 \equiv$ the leading edge tension and $T_2 \equiv$ the trailing edge tension ($T_2 > T_1$ for caret sails), it is required that

$$T_1 \leqslant T_{2.D} \leqslant T_2 .$$

Consider an extreme case, $T_1 = T_{2.D}$, for which, except at the leading edge, $T/T_{2.D} > 1$ and reaches a maximum at the trailing edge. At the trailing edge $\left(1+\frac{P'_r}{P'_{xz}}\right)$ is at a minimum (*see* Fig. 13g) but still exceeds unity: thus the value of $\frac{d\theta/ds}{(d\theta/ds)_{2.D}}\Bigg[= \left(1+\frac{P'_r}{P'_{xz}}\right)\Big/\frac{T}{T_{2.D}}\Bigg]$ may be less than, greater than or equal to unity. At the leading edge $\left(1+\frac{P'_r}{P'_{xz}}\right)$ is at a maximum (> 1) and $T/T_{2.D} = 1$, so that

$$\frac{d\theta/ds}{(d\theta/ds)_{2.D}} = \left(1+\frac{P'_r}{P'_{xz}}\right) > 1 .$$

In this case, conclusions regarding the profiles of caret and rectangular sails can only be drawn after fuller analysis, and would probably require evaluation of the integrals of equations (C.8); but consider the other extreme case, $T_2 = T_{2.D}$, for which except at the trailing edge $T/T_{2.D} < 1$ and reaches a minimum at the leading edge. At the trailing edge $\left(1+\frac{P'_r}{P'_{xz}}\right)$ is at a minimum (but > 1)

therefore $$\frac{d\theta/ds}{(d\theta/ds)_{2.D}} = \left(1+\frac{P'_r}{P'_{xz}}\right) > 1 ;$$

at the leading edge $\left(1+\frac{P'_r}{P'_{xz}}\right)$ is at a maximum (> 1) and $T/T_{2.D}$ at a minimum (< 1), so that

$$\frac{d\theta/ds}{(d\theta/ds)_{2.D}} > 1 \qquad \text{(in fact a maximum)},$$

but much more important

$$\frac{d\theta/ds}{(d\theta/ds)_{2.D}}\Bigg]_{t.e.} > \frac{d\theta/ds}{(d\theta/ds)_{2.D}}\Bigg]_{t.e.}$$

i.e. at the leading edge $d\theta/ds$ exceeds the two-dimensional value by a larger proportion than it does at the trailing edge (this proportion increasing monotonically along the chord). So in this case at least ($T_2 = T_{2.D}$), the upstream end of a caret sail will be of more pronounced curvature than the rectangular sail and the waves produced may be centred over larger extents of compression than was found in Figs. 6 to 9. It is not known whether this may be generalised to the statement that 'caret sails whose maximum chordwise tension does not exceed that of a rectangular sail producing the same net extent of compression, are likely to produce waves which are nearly centred over larger regions of that compression'; however the fact that some caret sails may produce closer approximations of Prandtl-Meyer flow could be useful in the design of, for example, intakes or nozzles for hypersonic or supersonic aircraft. This paper closes with comments on these and other applications in which two-dimensional or caret sails might be used.

5. *Applications.*

The rectangular sail whose profile is made adjustable, for example by control of the upper-surface pressure distribution, could be applied in the design of intakes producing some regions of isentropic compression. In Fig. 14a, the region between lines *A* and *B* could be constructed as a sail and any joints along these lines might appropriately be left unsealed so as to allow boundary layer bleed. For the caret intake of Fig. 14b, the anhedral form renders the problem of varying the geometry of the isentropic region far more difficult; however, for either type of intake the availability of two design Mach numbers for two-dimensional flows initiated by oblique shock waves[32] could be exploited with equal ease. It is also possible

that (as shown by shading in Figs. 14a and b), the cowl lip of either type of intake could be formed as a rectangular sail, pressurised by the internal flow and held in tension by a rigid lip extremity; the lip would probably incorporate leading-edge cooling but the cowl could be so thin that it might allow heat transferred from the internal flow to be radiated from the external surface of the cowl and so assist in cooling. For the caret intake, the pressure gradients on the isentropic surfaces are such as to suggest[32,34] that boundary-layer bleeds should be localised at the tip regions R, so that once more, sealing between the sail and the main body need not be provided.

Sail techniques might also be used in nozzles producing external expansion and of conventional or caret form; however, boundary-layer control would not normally be required in such applications.

A further application of the sail technique is shown in Fig. 14c. In the propulsive flow model chosen, the cowl is shown as a continuous foil running from intake to nozzle lip and stabilised in pure tension by the pressure difference which exists between the internal flow through the combustion chamber and nozzle, and the external flow over the cowl. If the internal flow comprises isentropic expansion downstream of constant pressure supersonic combustion, then the internal pressure distribution is as shown (*see* double-headed arrows); the external pressure on the cowl would gradually fall from that behind the shock S to that required to balance the pressure of the jet. The shaded area thus shows the pressure difference at any point and so, for a cowl at constant tension and of negligible weight, shows the manner in which $d\theta/ds$ would vary along the cowl; it is seen that the distribution of $d\theta/ds$ is consistent with the cowl shape shown, curvature being a maximum near the end of the combustion zone and zero at the nozzle lip. The possibility of building the cowl and lower side of the combustion chamber as a single, heat resistant foil, would allow the upper side(s) of the combustion chamber(s) to be built as hollow(s) in the main body B, rather than as actual duct(s); as shown in the sketch inset in Fig. 14c, such hollows could also be constructed as curved foils under tension, and their positioning relative to the cowl would allow for combustion chambers having (perhaps variable) divergence.

For use with purely lifting bodies giving high values of L/D, curved surfaces which weaken or eliminate leading-edge shock waves tend to produce an excessive skin friction and low lift on their upstream ends (*see* work by Fetterman as cited by Becker[35]); at a given C_L such bodies may therefore offer little improvement, or even some loss, in L/D. Even in non-viscous flow the lifting performance of isentropic sails (*see* Fig. 6c) is liable to be worse than that of a simple, two-dimensional wedge. However, a conventionally shaped body may necessitate the use of conventional structural techniques and so involve structure weights in excess of (say) 5 to 10 lb/ft^2. If, by the use of sails (in either two-dimensional or caret form), local structure weights can be reduced to the order of even the worst in Fig. 10, this great improvement in local structure weight might well outweigh any falls in aerodynamic efficiency as reflected in L/D. For the simple case of cruising flight, the problem would be to increase the value of $\left(\frac{L}{D}\log_e\frac{W_1}{W_2}\right)$ so that, for a given fuel allowance and specific fuel consumption, the range $\left(=\frac{V}{S.F.C.}\frac{L}{D}\log_e\frac{W_1}{W_2}\right)$ would be increased; that is, the problem would only be solved if the weight saved locally by replacing conventional structures with sails, more than compensated for the combined effects of reduced aerodynamic efficiency and the weight of spars and booms etc. added specifically for tethering and controlling the membrane. Of course, savings in overall weight may depend not only on minimising local weights, but also on maximising the area of those regions of a vehicle to which weight-saving techniques may be applied; thus consideration of configuration design is intrinsically required. Tentative suggestions for purely lifting systems are now described.

In Section 3.2 it was shown that the lifting characteristics of isentropic sails could be substantially worse than those of simple wedges. However it is at least possible that a sail in combination with a wedge spar might combine a reasonable aerodynamic performance with a robust structure of low total weight. If so it is possible that the flow of Fig. 15a could be produced beneath the wing of an aircraft such as that of Fig. 15b, the trailing edge of the sail being attached to a rigid spar. Alternatively the trailing edge might be attached to a tensioned cable as in Fig. 15c. In either case, variable wing area could possibly be achieved during the acceleration phase by moving the trailing edge to the position shown dotted and stowing some

of the sail inside the wedge-spar, the full area being available for cruise or landing and/or take-off; a further possibility is that at low speeds the sail could be used as a large flap over which propulsive jets, exhausted from power units inside the wedge-spar or the main body, might produce significant lift forces. The sail-flap's centre of lift could be much closer to the aircraft centre of gravity than in the case of flap-blown delta wings of conventional type, and so pitching problems might be avoided.

It is also possible that the lifting flow of Fig. 15a could be produced by the composite lifting system of Fig. 16; in Fig. 16a a shock wave is produced not by a wedge-spar but by a cylindrical parawing P (*see* Fig. 1b), whose tip is tethered to the end of the wedge-spars of the sail S, these spars being joined at T and thus being mutually braced at least against forces which act in a dragwise sense. That this type of composite sail system would be particularly suited to 'waverider' vehicles of integrated form[32], is shown in Fig. 16b.

Finally Daskin and Feldman[17], and Boyd[20,21], have suggested that for adequate strength under some conditions, sail membranes should be of woven wire; with such membranes[36-38], porosity would effectively result unless a sealant were applied to the membrane[36], so that

(1) boundary layers might be removable over at least some parts of a compression surface, and

(2) since, as shown by Boyd[22], porosity effectively produces local reductions in incidence, it could be treated as a form of variable geometry.

6. *Conclusions.*

For free-stream Mach numbers between 10 and 14, rectangular sails in pure tension and of finite weight are shown to produce two-dimensional isentropic compression waves; for the higher free-stream Mach numbers, the down-stream parts of these waves are nearly centred (for example, for $M_\infty = 10$ and $M_{comp} = 3{\cdot}5$, that part of the wave in which the flow is compressed from about $M = 7$ to $M_{comp} = 3{\cdot}5$ is nearly centred). At a given free-stream Mach number, an increase in upper-surface pressure or sail weight usually increases the gaps between initial compression waves and the near-focus of later waves; if a wedge-spar is attached to the leading edge of a sail, an increase in wedge angle appears to reduce the influence of upper surface pressure and sail weight on sail profile and wave form. Investigation of the structural aspects of two-dimensional sails suggests that, even for long sails (e.g. 100 ft chord) at high Mach number (e.g. 10) and low stress (e.g. 5 tons/in^2), the weight of the membrane need not exceed 1 lb/ft^2.

Since rectangular sails appear to yield simultaneously a useful type of supersonic flow and promising values of membrane weight, the study is extended to 'caret' sails, which allow leading edges to be swept, which can in principle produce and contain two-dimensional waves, and to which single (though not necessarily conical) curvature imparts a stiffness-due-to-shape. It is found that for the equilibrium of an element of such a sail only tensile forces are required, firstly, tensions directed along the chord of the sail and, secondly, tensions acting from tip to root along local generators of the singly curved surface. Application of appropriate tensions can therefore reduce (to zero if necessary) the extent to which the intrinsic stiffness of a caret sail is exploited. Alternatively, to simplify the loading system, a sail may be operated in such a way that it retains its shape at least partly by reason of its intrinsic stiffness. Such a device might find application in the design of supersonic or hypersonic vehicles. Various applications are explored, for both rectangular and caret sails, including wings, intakes, cowls and nozzles.

Acknowledgement.

The author is indebted to Mrs. M. G. Joyce, who programmed the Mercury Computer and produced all the data presented in this Report.

LIST OF SYMBOLS

A, B	Defined for equations (5) and (B.6)
c_f	Skin-friction coefficient
C_L	Lift coefficient
D	Drag force
k	$= \sqrt{\frac{\gamma-1}{\gamma+1}} \left(= \frac{1}{\sqrt{6}} \text{ if } \gamma = 1{\cdot}4 \right)$
K	Constant defined in Appendix C
L	Lift force
M	Mach number
p	Static pressure
p_T	Stagnation pressure
P	Elemental forces in Figs. 11 and 13
$(P.D.)$	Pressure difference
q_∞	Kinetic pressure of free-stream
r	Radius vector in polar co-ordinate system } *See* Fig. 3
r_0	Value of r at sonic conditions } *See* Fig. 3
s	Arc length
t	Sail thickness
T	Static temperature
T	Sail tension per unit span
V	Flow velocity
w	Sail weight per unit wetted area
x, x'	Orthogonal co-ordinates defined in text
y, y'	Orthogonal co-ordinates defined in text
z, z'	Orthogonal co-ordinates defined in text
β	$= \sqrt{M^2-1}$
γ	Ratio of specific heats (c_p/c_v), (= 1·4 for air)
η_{KE}	Kinetic-energy efficiency of shock wave
θ	Defined in Figs. 3 and 5
θ_c	Angle of climb
Θ	Deflection of flow at sail leading edge or wedge spar
κ	Cross-flow in boundary layer

μ $= \sin^{-1}\frac{1}{M} \equiv$ Mach angle

ν $= \frac{1}{k}\tan^{-1} k\beta - \tan^{-1}\beta \equiv$ Prandtl-Meyer angle $= \phi + \mu - 90°$

ρ Flow density

τ *See* Fig. 13c

ϕ $= \frac{1}{k}\tan^{-1} k\sqrt{M^2-1}$. *See* Fig. 3 and Appendix A

ψ $= \tan^{-1}(r\, d\phi/dr)$. *See* Fig. 3 and Appendix A

Subscripts

1 Refers to conditions immediately downstream of the shock wave from the wedge-spar (*see* Fig. 5a)

o Refers to sonic conditions

u Refers to upper surface of sail

l Refers to lower surface of sail

N Refers to component (i.e. of Mach number) normal to shock wave

∞ Refers to free-stream conditions

comp Refers to conditions at sail trailing edge

REFERENCES

No.	*Author(s)*	*Title, etc.*
1	B. Thwaites	The aerodynamic theory of sails. Part 1 Two-dimensional sails. *Proc. R. Soc. Lond.* Series A, *261*, 1306, 402–422, 1961.
2	J. N. Nielsen	Theory of flexible aerodynamic surfaces. *J. appl. Mech.*, *30*, Series E, 3, 435–442, 1963.
3	E. A. Boyd	Aerodynamic characteristics of a hypersonic parachute. COA Rept. No. 152, 1961. ARC 23360.
4	H. G. Heinrich	A supersonic parachute based on the inlet diffuser concept. AGARD Rept. 445, 1963.
5	S. A. Tancredi	Parachute technology. Defense Documentation Centre. AD 427014, 1964.
6	F. M. Rogallo and J. G. Lowry	Flexible re-entry gliders. S.A.E. Preprint No. 175C, 1960.
7	F. M. Rogallo, J. G. Lowry, .. D. R. Croom and R. T. Taylor	Preliminary investigation of a paraglider. NASA TN D–443, 1960.
8	R. T. Taylor	Wind-tunnel investigation of paraglider models at supersonic speeds. NASA TN D–985, 1961.
9	P. G. Fournier and B. A. Bell	Transonic pressure distributions on three rigid wings simulating paragliders with varied canopy curvature and leading-edge sweep. NASA TN D–1009, 1962.
10	J. A. Penland	A study of the aerodynamic characteristics of a fixed geometry paraglider configuration and three canopies with simulated variable canopy inflation at a Mach number of 6·6. NASA TN D–1022, 1962.
11	P. G. Fournier..	Pressure distributions on three rigid wings simulating parawings with varied canopy curvature and leading-edge sweep at Mach numbers from 2·29 to 4·65. NASA TN D–1618, 1963.
12	D. E. Wornom and .. .. R. T. Taylor	Aerodynamic characteristics of a flexible-canopy paraglider model at a Mach number of 4·5 for angles of attack to 360° and sideslip angles from 0° to 90°. NASA TN D–1776, 1963.
13	C. Briggs	An annotated bibliography on paragliders. Library Literature Search No. 24, Martin Co., Denver, U.S.A., 1963, P.121815. AD 295,143.

REFERENCES—*continued*

No.	*Author(s)*	*Title, etc.*
14	R. W. Fralich	Stress and shape analysis of a paraglider wing. A.S.M.E. 64–WA/AV–4, 1964.
15	G. I. Maikapar	On the wave drag of axisymmetric bodies at supersonic speeds. Russian *J. App. Math. Mech.* (Pergamon Translation) *23*, 2, 528–531, 1959.
16	T. R. F. Nonweiler	Delta wings of shapes amenable to exact shock-wave theory. *Jl. R. aeronaut. Soc., 67*, 625, 39–40, 1963.
17	W. Daskin and L. Feldman . .	The characteristics of two-dimensional sails in hypersonic flow. *J. Ae. Sci., 25*, 53–55, 1958.
18	L. Lees	Laminar heat transfer over blunt nosed bodies at hypersonic flight speeds. Jet Propulsion, *26*, 4, 1956.
19	M. R. Fink	Analytical study of the aerodynamic performance and geometric shape of two-dimensional sails in supersonic flow. United Aircraft Corporation Report M–1275–1, 1959.
20	E. A. Boyd	Busemann correction to the characteristics of the two-dimensional hypersonic sail. COA Report No. 140, ARC 22499, 1960.
21	E. A. Boyd	The characteristics of a two-dimensional supersonic sail. COA Report No. 143, ARC 22647, 1960.
22	E. A. Boyd	Effect of porosity on the two-dimensional supersonic sail. *J. aero. Space. Sci., 29*, 232–3, 1962.
23	E. A. Boyd	Shape of the porous two-dimensional hypersonic sail. *AIAA Journal 1*, 5, 1177–1178, 1963.
24	N. H. Johannesen	Experiments on two-dimensional supersonic flow in corners and over concave surfaces. Fluid Motion Lab., Univ. of Manchester. ARC 14,607, 1952.
25	J. F. Connors, R. R. Woollett and R. E. Blue	Interferometric observation of flow about an isentropic (reverse Prandtl-Meyer streamline) compression wedge at Mach 3·0. NACA RM E55A28, 1955, NACA/TIB/4639.
26	D. R. Chapman, D. M. Kuehn and H. K. Larson	Preliminary report on a study of separated flows in supersonic and subsonic streams. NACA RM A55L14, TIL 4968, 1956.
27	D. R. Chapman, D. M. Kuehn and H. K. Larson	Investigation of separated flows in supersonic and subsonic streams with emphasis on the effect of transition. NACA TN 3869, 1957

REFERENCES—*continued*

No.	*Author(s)*	*Title, etc.*
28	D. M. Kuehn	Experimental investigation of the pressure rise required for the incipient separation of turbulent boundary layers in two-dimensional supersonic flow. NASA Memo 1–21–59A, NASA TIL 6209, 1959.
29	J. R. Sterrett and J. C. Emery	Experimental separation studies for two-dimensional wedges and curved surfaces at Mach numbers of 4·8 to 6·2. NASA TN D–1014, 1962.
30	A. Ferri..	Review of problems in application of supersonic combustion. *Jl. R. aeronaut. Soc., 68*, 645, 575–597, 1964.
31	J. Pike	Private communication from R.A.E., Bedford, 1965.
32	L. H. Townend	On lifting bodies which contain two-dimensional supersonic flows. ARC R. & M. No. 3383, 1963.
33	R. W. Hess	An experimental study of the flutter of sails having a delta planform tested from a Mach number of 0·1 to a Mach number of 1·9. NASA TM X–355, 1961.
34	J. C. Cooke and O. K. Jones ..	The boundary layer on a Townend surface. *Aeronaut. Q. 16*, 5, Part 2, 145–158, 1965.
35	J. V. Becker	Studies of high lift-drag ratio hypersonic configurations. AIAA Paper No. 64–551, presented to Fourth I.C.A.S. Congress, 1964.
36	D. Hritzay and R. Wiant ..	Wire cloth structure for a radiating re-entry vehicle. AVCO Everett Research Lab. Rept. No. 123, AD 275, 105, P113482, 1962.
37	J. H. Ross	Unique flexible fibrous materials for decelerators. Proceedings of Symposium on Parachute Technology and Evaluation, FTC–TDR–64–12, *2*, 420–433, 1964.
38	M. G. Kurz	Transpiration cooling through RIGIMESH sintered woven-wire sheet. Aircraft Porous Media Inc., Field Services Report 18B, 1964.
39	J. C. Cooke	Private communication, 1965.

APPENDIX A

The Equilibrium of Membranes in Constant Tension.

Consider the flexible membrane sketched in Fig. 3 to be of unit width and of zero weight and to be statically inflated at constant tension T, to a profile given by $\phi = \phi(r)$. The required distribution of pressure difference (*P.D.*) across the membrane is found as follows:

$$P.D. = T\frac{d\theta}{ds}$$

$$ds^2 = dr^2 + r^2 . d\phi^2$$

$$\tan\psi = r\frac{d\phi}{dr}$$

$$\phi + \psi - \theta = \text{constant}$$

therefore

$$\frac{P.D.}{T} = \frac{d\phi + d\psi}{ds} = \left[\frac{d\phi}{dr} + \frac{d}{dr}\tan^{-1}\left(r\frac{d\phi}{dr}\right)\right] \Big/ \sqrt{1 + r^2\left(\frac{d\phi}{dr}\right)^2} \tag{A.1}$$

or

$$\frac{P.D.}{T} = \left[1 + \frac{d}{d\phi}\tan^{-1}\left(r\frac{d\phi}{dr}\right)\right] \Big/ \sqrt{r^2 + \left(\frac{dr}{d\phi}\right)^2}. \tag{A.2}$$

These are general equations for the pressure difference required to maintain a flexible, weightless membrane in any shape given by $\phi = \phi(r)$.

Consider the case when the membrane is required to take up a shape identical with that of a streamline in a centred, isentropic wave i.e. a Prandtl-Meyer corner flow. For this flow, $\psi = \mu$,

therefore

$$r\frac{d\phi}{dr} = \tan\psi = \tan\mu = 1/\sqrt{M^2 - 1} \tag{A.3}$$

Also for continuity of mass flow between for example a station at which the flow area $\equiv A = A_0$ and $M = 1$, and a station at which $A > A_0$ and $M > 1$, it is required that $\rho_0 A_0 V_0 = \rho A V$.

But if in the polar co-ordinate system of Fig. 3, O is the centre of isentropic expansion (or compression), then A_0 and A correspond respectively to r_0 and $r \sin\mu$

therefore

$$\frac{\rho_0}{\rho} = \frac{A}{A_0}\frac{V}{V_0} = \left[\frac{r\sin\mu}{r_0}\frac{M}{1}\sqrt{\frac{\gamma R T}{\gamma R T_0}}\right] = \frac{r}{r_0}\sqrt{\frac{T}{T_0}}$$

therefore

$$\frac{r}{r_0} = \frac{p_0}{p}\sqrt{\frac{T_0}{T}} = \frac{p_0}{p}\sqrt{\frac{T}{T_0}} = \left(\frac{2+(\gamma-1)M^2}{\gamma+1}\right)^{\frac{\gamma+1}{2(\gamma-1)}} \quad \text{for isentropic flow.} \tag{A.4}$$

It follows that $\left(\frac{1}{r}\frac{dr}{dM}\right) = \frac{(\gamma+1)M}{2+(\gamma-1)M^2}$, so that from equation (A.3)

$$\int d\phi = \int \left(\frac{1}{r}\frac{dr}{dM}\right)\frac{dM}{\sqrt{M^2-1}} = \int \frac{(\gamma+1)}{2+(\gamma-1)M^2}\, d\sqrt{M^2-1}$$

therefore

$$\phi + c = \sqrt{\frac{\gamma+1}{\gamma-1}}\tan^{-1}\sqrt{\frac{\gamma-1}{\gamma+1}(M^2-1)}\,;$$

but for $\phi = 0, M = 1$ therefore $c = 0$, and if $k \equiv \sqrt{\frac{\gamma-1}{\gamma+1}}$,

$$\phi = \frac{1}{k}\tan^{-1} k\sqrt{(M^2-1)} \text{ i.e. } M^2 = 1+\frac{1}{k^2}\tan^2 k\phi\,. \tag{A.5}$$

Thus in equation (A.4)

$$\frac{r}{r_0} = 1/\cos^{1/k^2} k\phi\,. \tag{A.6}$$

This is an equation for a streamline in Prandtl-Meyer corner flow; thus for a membrane held in pure tension to such a profile,

$$\phi = \phi(r) = \frac{1}{k}\cos^{-1}\left(1\Big/\left(\frac{r}{r_0}\right)^{k^2}\right), \tag{A.7}$$

and the required distribution of pressure difference is found from equations (A.7) and (A.1) (or (A.2)),

$$\frac{(P.D.)\,r_0}{T} = \left(\frac{1}{k^2}-1\right)\frac{\tan^2 k\phi\,.\cos^{1/k^2} k\phi}{\left(1+\frac{1}{k^2}\tan^2 k\phi\right)^{3/2}} = \left(\frac{1}{k^2}-1\right)f(k\phi) \tag{A.8}$$

APPENDIX B

The Statics of Rectangular Sails in Isentropic Flow.

Non-Viscous flow.

In Fig. 5a, the sail is assumed to be

(1) subject to negligible tensions due to skin friction,

(2) subject to negligible increments in pressure due to sail porosity or boundary-layer thickness or separation,

(3) of negligible stiffness; further

(4) γ is assumed constant.

For equilibrium of an element of such a sail, the forces in Fig. 5b must satisfy the two requirements:

$$T \,.\, dy \cos\frac{d\theta}{2} = (T+dT)\, dy \cos\frac{d\theta}{2} + w \,.\, ds \,.\, dy \,.\, \sin(\theta+\theta_c) \tag{B.1}$$

and

$$(2\,T+dT)\, dy \sin\frac{d\theta}{2} + w \,.\, ds \,.\, dy \,.\, \cos(\theta+\theta_c) = (p_l - p_u)\, ds \,.\, dy \tag{B.2}$$

from which it follows that

$$\frac{dT}{ds} = -w \,.\, \sin(\theta+\theta_c)$$

and

$$T\frac{d\theta}{ds} = p_l - (p_u + w \,.\, \cos(\theta+\theta_c)) \,.$$

For sails with which tension is large in comparison with the weight of the sail, dT/ds can be ignored, i.e. tension can be taken as constant. On such a sail, at a point such as P in Fig. 5a:

$$T\frac{d\theta}{ds} = p_l - (p_u + w\cos(\theta+\theta_c)) \tag{B.3}$$

$$p_l = p_{T1}\left(1+\frac{\gamma-1}{2}M^2\right)^{-\frac{\gamma}{\gamma-1}},\quad ds = dx/\cos\theta = dy/\sin\theta \tag{B.4}$$

therefore

$$\cos\theta \,.\, d\theta = \frac{p_{T1}\, dx}{T}\left[\left(1+\frac{\gamma-1}{2}M^2\right)^{-\frac{\gamma}{\gamma-1}} - \frac{p_u + w \,.\, \cos(\theta+\theta_c)}{p_{T1}}\right]$$

$$\sin\theta \,.\, d\theta = \frac{p_{T1}\, dy}{T}\left[\left(1+\frac{\gamma-1}{2}M^2\right)^{-\frac{\gamma}{\gamma-1}} - \frac{p_u + w \,.\, \cos(\theta+\theta_c)}{p_{T1}}\right].$$

Also $$\theta = \Theta + (\nu_1 - \nu)$$

therefore $$d\theta = -d\nu = \left(\frac{1}{1+\beta^2} - \frac{1}{1+k^2\beta^2} \right) d\beta ,$$

in which

$$\beta = \sqrt{M^2-1}\,, k = \sqrt{\frac{\gamma-1}{\gamma+1}}\,, \nu = \frac{1}{k}\tan^{-1} k\beta - \tan^{-1}\beta .$$

The profile of the sail is thus:

$$\frac{p_{T1}}{T}\int_0^x dx = \int_{\beta_1}^{\beta} \frac{A}{B}.\cos\theta\,.\,d\beta \tag{B.5}$$

$$\frac{p_{T1}}{T}\int_0^y dy = \int_{\beta_1}^{\beta} \frac{A}{B}.\sin\theta\,.\,d\beta \tag{B.6}$$

in which

$$A = \left(\frac{1}{1+\beta^2} - \frac{1}{1+k^2\beta^2} \right), \beta^2 = M^2-1\,, \beta_1^2 = M_1^2-1\,,$$

$$B = \left[\left(1+\frac{\gamma-1}{2}M^2 \right)^{-\frac{\gamma}{\gamma-1}} - \frac{p_u + w\cos(\theta+\theta_c)}{p_{T1}} \right],$$

$$\theta = \Theta + \frac{1}{k}\tan^{-1} k\,\beta_1 - \tan^{-1}\beta_1 - \frac{1}{k}\tan^{-1} k\,\beta + \tan^{-1}\beta\,,$$

$$\frac{p_u + w\cos(\theta+\theta_c)}{p_{T1}} = \frac{(p_u/p_\infty) + (w/p_\infty)\cos(\theta+\theta_c)}{(p_{T1}/p_{T_\infty})\,(p_{T_\infty}/p_\infty)},$$

$$\frac{p_{T1}}{p_{T_\infty}} = \left[\frac{(\gamma+1)M_N^2}{2+(\gamma-1)M_N^2} \right]^{\frac{\gamma}{\gamma-1}} \left[\frac{\gamma+1}{2\gamma M_N^2 - (\gamma-1)} \right]^{\frac{1}{\gamma-1}},$$

$$\frac{p_{T_\infty}}{p_\infty} = \left(1+\frac{\gamma-1}{2}M_\infty^2 \right)^{\frac{\gamma}{\gamma-1}}.$$

Viscous flow

Suppose now that a skin-friction force acts on the sail of Fig. 5a, and that the friction drag on one side of an element such as that of Fig. 5b is equal to $(q_\infty\,.\,c_f\,.\,ds\,.\,dy)$. Then equation (B.1) becomes

$$T\,.\,dy\,.\cos\frac{d\theta}{2} = (T+dT)\,dy\,.\cos\frac{d\theta}{2} + w\,.\,ds\,.\,dy\,.\sin(\theta+\theta_c) + q_\infty\,.\,c_f\,.\,ds\,.\,dy$$

and if $w\,.\sin(\theta+\theta_c)$ is neglected (as above), the equations of equilibrium are then

$$\frac{dT}{ds} = -q_\infty \cdot c_f \tag{B.7}$$

$$T\frac{d\theta}{ds} = p_l - (p_u + w \cdot \cos(\theta + \theta_c)). \tag{B.8}$$

So

$$-q_\infty \cdot c_f = [p_l - (p_u + w \cdot \cos(\theta+\theta_c))]\ \frac{d\theta}{ds}\ \frac{d}{d\theta}\left(\frac{ds}{d\theta}\right) + \frac{ds}{d\theta}\ \frac{d}{ds}[p_l - (p_u + w \cdot \cos(\theta+\theta_c))]$$

therefore

$$-\frac{q_\infty\, c_f + \dfrac{d}{d\theta}[p_l - (p_u + w\cos(\theta+\theta_c))]}{[p_l - (p_u + w\cos(\theta+\theta_c))]} = \frac{d\theta}{ds}\ \frac{d}{d\theta}\left(\frac{ds}{d\theta}\right)$$

therefore

$$-\int \frac{q_\infty\, c_f + \dfrac{d}{d\theta}[p_l - (p_u + w\cos(\theta+\theta_c))]}{[p_l - (p_u + w\cos(\theta+\theta_c))]}\, d\theta \equiv I = \log_e\left(k''\frac{ds}{d\theta}\right) \tag{B.9}$$

therefore

$$\frac{ds}{d\theta} = \frac{1}{k''}\exp(I) = \frac{dx}{\cos\theta \cdot d\theta} = \frac{dy}{\sin\theta \cdot d\theta}\ (k'' = \text{const.}). \tag{B.10}$$

So the sail profile is given by:

$$\left.\begin{aligned} k''\int dx &= \int \exp(I)\cdot\cos\theta\cdot d\theta \\ k''\int dy &= \int \exp(I)\cdot\sin\theta\cdot d\theta \end{aligned}\right\} d\theta = \left(\frac{1}{1+\beta^2} - \frac{1}{1+k^2\beta^2}\right)d\beta = A\cdot d\beta$$

in which k'' can be evaluated as follows.

From (B.8) and (B.9)

$$\therefore k'' = \exp(I)\cdot\frac{d\theta}{ds} = \exp(I)\cdot\frac{[p_l - (p_u + w\cos(\theta+\theta_c))]}{T}$$

i.e. at a point on the sail where $s = s''$, $\theta = \theta''$, $T = T''$, $p_l = p_l''$,

$$k''\quad \frac{p_l'' - (p_u + w\cos(\theta''+\theta_c))}{T''}\quad \exp\left[-\int_{\theta}^{\theta''} \frac{q_\infty\, c_f + \dfrac{d}{d\theta}[p_l - (p_u + w\cos(\theta+\theta_c))]}{[p_l - (p_u + w\cos(\theta+\theta_c))]}\, d\theta\right]$$

or at the leading edge of the sail, $M = M_1, v = v_1, \theta = \Theta$,

$$p_l'' = p_{T1}\left(1+\frac{\gamma-1}{2}M_1^2\right)^{-\frac{\gamma}{\gamma-1}}, T = T_1, \exp(I) = 1/e^{\circ} = 1,$$

therefore

$$k'' = \frac{p_{T1}}{T_1}\left[\left(1+\frac{\gamma-1}{2}M_1^2\right)^{-\frac{\gamma}{\gamma-1}} - \frac{p_u + w\cos(\Theta+\theta_c)}{p_{T1}}\right]. \tag{B.11}$$

Thus

$$\frac{p_{T1}\,x}{T_1} = \int_{\beta_1}^{\beta} \frac{\exp(I).A.\cos\theta.\,d\beta}{\left(1+\frac{\gamma-1}{2}M_1^2\right)^{-\frac{\gamma}{\gamma-1}} - \frac{p_u + w\cos(\Theta+\theta_c)}{p_{T1}}} \tag{B.12}$$

and

$$\frac{p_{T1}\,y}{T_1} = \int_{\beta_1}^{\beta} \frac{\exp(I).A.\sin\theta.\,d\beta}{\left(1+\frac{\gamma-1}{2}M_1^2\right)^{-\frac{\gamma}{\gamma-1}} - \frac{p_u + w\cos(\Theta+\theta_c)}{p_{T1}}} \tag{B.13}$$

in which

$$\theta = \Theta + \frac{1}{k}\tan^{-1} k\beta_1 - \tan^{-1}\beta_1 - \frac{1}{k}\tan k\beta + \tan^{-1}\beta.$$

That (B.12) and (B.13) reduce to the integrals of (B.5) and (B.6) can be shown as follows. If

$$c_f = 0, \exp(I) = \exp\left(-\log_e k'\left[p_l - (p_u + w\cos(\theta+\theta_c))\right]\right): \tag{B.14}$$

thus in equation (B.9)

$$\log_e\left(k''\frac{ds}{d\theta}\right) = -\log_e k'\left[p_l - (p_u + w\cos(\theta+\theta_c))\right],$$

and from equation (B.8),

$$k'\left[p_l - (p_u + w\cos(\theta+\theta_c))\right] = \frac{1}{k''}\frac{d\theta}{ds} = \frac{\left[p_l - (p_u + w\cos(\theta+\theta_c))\right]}{k''\,T}.$$

It follows that in equation (B.9),

$$\log_e(k''\,ds/d\theta) = -\log_e k'\left[p_l - (p_u + w\cos(\theta+\theta_c))\right],$$

and from equation (B.8), that

$$k'\left[p_l - (p_u + w\cos(\theta+\theta_c))\right] = \frac{1}{k''}\frac{d\theta}{ds} = \frac{\left[p_l - (p_u + w\cos(\theta+\theta_c))\right]}{k''\,T}.$$

Thus equation (B.14) becomes,

$$\exp(I) = k'' \, T/[p_l - (p_u + w \, . \cos(\theta + \theta_c))] \, ,$$

and from (B.11)

$$\exp(I) = \left[\frac{\left(1 + \frac{\gamma - 1}{2} M_1^2\right)^{-\frac{\gamma}{\gamma - 1}} - \frac{p_u + w \cos(\Theta + \theta_c)}{p_{T1}}}{\left(1 + \frac{\gamma - 1}{2} M^2\right)^{-\frac{\gamma}{\gamma - 1}} - \frac{p_u + w \cos(\theta + \theta_c)}{p_{T1}}} \right]. \tag{B.15}$$

Substitution of equation (B.15) into the integrals of (B.12) and (B.13) leads to those of (B.5) and (B.6).

APPENDIX C

The Statics of Caret Sails in Isentropic Flow.

The pressure forces acting on a singly curved caret sail are shown in Fig. 13a. Those components which lie in a plane parallel to $x'\,Oz'$ are drawn in Fig. 13b from which it is seen that

$$\left.\begin{aligned} P'_r &= P_r \sin\mu = P_r/M \\ P''_r &= P_r \cos\mu = P_r\sqrt{(M^2-1)}/M \end{aligned}\right\} \text{ i.e. } \frac{P''_r}{P'_r} = \sqrt{M^2-1}\,.$$

From Fig. 13c,

$$P_r = P'_y\,.\cot\tau$$

and

$$P'_y = (p_l - p_u)\,dA'_y = (p_l - p_u)\cot\tau\,.\sin\mu\,.\,ds\,.\,dy'\,.$$

But

$$P'_{xz} = (p_l - p_u)\,ds\,.\,dy'\,, \tag{C.1}$$

therefore

$$P'_y = P'_{xz}\cot\tau\,.\sin\mu\,, P_r = P'_{xz}\cot^2\tau\,.\sin\mu\,. \tag{C.2}$$

From Fig. 13d it is seen that for centred or non-centred compression (i.e. for singly but not necessarily conically curved sails)

$$r\tan\tau = r_1\tan\tau_1$$

therefore

$$\frac{P_r}{P'_{xz}} = \left(\frac{r}{r_1}\right)^2\cot^2\tau_1\,.\sin\mu\,.$$

But from Fig. 13e, $\cot\tau_1 = \cot\tau_\infty \sin(\zeta-\delta)/\sin\mu_1$;

also

$$\left(\frac{r}{r_1}\right)^2 = \left(\frac{r}{r_0}\,\frac{r_0}{r_1}\right)^2 = \left(\frac{\cos\left(\tan^{-1}k\sqrt{M_1^2-1}\right)}{\cos\left(\tan^{-1}k\sqrt{M^2-1}\right)}\right)^{2/k^2} = \left(\frac{1+k^2(M^2-1)}{1+k^2(M_1^2-1)}\right)^{1/k^2},$$

$$\sin^2(\zeta-\delta) = \frac{1}{M_1^2}\,\frac{2+(\gamma-1)M_N^2}{2\gamma M_N^2-(\gamma-1)}, \sin^2\mu_1 = \frac{1}{M_1^2}, \cos\tau_\infty = \frac{\sin\Lambda}{\cos\zeta}.$$

Thus,

$$\frac{P_r}{P'_{xz}} = \left(\frac{2+(\gamma-1)M_N^2}{2\gamma M_N^2-(\gamma-1)}\right)\frac{\sin^2\Lambda}{\cos^2\zeta-\sin^2\Lambda}\left(\frac{1+k^2(M^2-1)}{1+k^2(M_1^2-1)}\right)^{1/k^2}\frac{1}{M}$$

$$= K\frac{(1+k^2(M^2-1))^{1/k^2}}{M}$$

in which $K = f(\gamma, M_N, \Lambda, M_\infty)$ and for zero sweep (rectangular sails), $K = 0 = \dfrac{P_r}{P'_{xz}}$.

So:

$$\left.\begin{aligned}\frac{P'_r}{P'_{xz}} &= \frac{1}{M}\frac{P_r}{P'_{xz}} = K\frac{(1+k^2(M^2-1))^{1/k^2}}{M^2} = \frac{K}{M^2}\left(\frac{r}{r_0}\right)^2\\ \frac{P''_r}{P'_{xz}} &= \sqrt{M^2-1}\,\frac{P'_r}{P'_{xz}} = \frac{K}{M^2}\sqrt{M^2-1}\left(\frac{r}{r_0}\right)^2\end{aligned}\right\} \qquad \text{(C.3)}$$

Equations (C.1) and (C.2) relate those components of pressure force (on element E of a caret sail) which lie in a plane parallel to $x'Oz'$. The other component is P_g which, as shown from geometrical arguments in Section 4.2, is directed along the surface generator through the centroid of element E; thus

$$P_g = P'_y \operatorname{cosec}\tau = P_r \sec\tau = K\frac{(1+k^2(M^2-1))^{1/k^2}}{M}\,.\,P'_{xz}\,.\,\sec\tau\,,$$

so from (C.1)

$$P_g = \frac{K}{M}\left(\frac{r}{r_0}\right)^2 (p_l-p_u)\,ds\,.\,dy'\,.\,\sec\tau\,.$$

If a tension is applied to resist this force P_g, such that $T_g \equiv$ tension per unit (arc) length of chord, then

$$T_g\,.\,ds = P_g\,;$$

thus, the net tension per unit (arc) length of root chord, to be applied parallel to the local generator of the singly curved surface (so as to balance the sum of those components of pressure force which act along that generator), is given by

$$\sum_{\text{gen}} T_g \equiv T_{g_{\text{root}}}\,,$$

i.e.

$$T_{g_{\text{root}}} = \int_{y'_1}^{y'_2} \frac{K}{M}\left(\frac{r}{r_0}\right)^2 (p_l-p_u)\sec\tau\,.\,dy'\,.$$

But along a generator M, r/r_0, p_l and τ are constant, p_u is in this analysis assumed constant and $K = f(\gamma, M_N, \Lambda, M_\infty)$; thus

$$T_{g_{root}} = \frac{K}{M}\left(\frac{r}{r_0}\right)^2 (p_l - p_u) \sec\tau \,.\, (y'_2 - y'_1)$$

in which $(y'_2 - y'_1)$ = span of sail (i.e. the length from tip to root projected onto Oy' as in Fig. 13f).

The components of pressure force acting on element E, that is, $(P'_{xz} + P'_r)$, P''_r and P_g can be calculated as above; of these three forces

(1) $(P'_{xz} + P'_r)$ can be balanced by tensions acting in a plane parallel to $x'Oz'$,

(2) P''_r contributes to the tangential forces and so to the value of $\dfrac{dT}{ds}$ and

(3) P_g can be achieved by a tensile force acting along the local generator, and the sum of the P_g-components along a given generator can be balanced (at the root) by a single tensile force of magnitude $T_{g_{root}}$.

If it is assumed that such a force $(T_{g_{root}})$ is applied to a caret sail, then since the two remaining forces P''_r and $(P'_r + P'_{xz})$ lie in a single plane, the calculation of the tensions required to balance them is a problem in two dimensions only; the equilibrium equations are therefore modified forms of (B.1) and (B.2), modifications arising from the existence of boundary-layer cross-flow[32,34], the inclusion of P'_r and P''_r, and the fact that weight and skin friction are based on the wetted area of element E, which from Fig. 13c is seen to be $\left(ds \,.\, dy' \,.\, \sqrt{1+\cot^2\tau \,.\, \sin^2\mu}\right)$. So:

$$T \,.\, dy' \,.\, \cos\frac{d\theta}{2} + P''_r = (T + dT)\, dy' \cos\frac{d\theta}{2} + (w \,.\, \sin(\theta+\theta_c) + q_\infty \,.\, c_f \cos\kappa)\, ds\, dy' \sqrt{1+\cot^2\tau \,.\, \sin^2\mu}$$

$$(2T + dT)\, dy' \,.\, \sin\frac{d\theta}{2} + w \,.\, \cos(\theta+\theta_c) \,.\, ds \,.\, dy' \,.\, \sqrt{1+\cot^2\tau \,.\, \sin^2\mu} = P'_{xz}\left(1 + \frac{P'_r}{P'_{xz}}\right)$$

which from equations (C.1), (C.2), (C.3) become

$$\frac{dT}{ds} = (p_l - p_u)\frac{K}{M^2}\left(\frac{r}{r_0}\right)^2 \sqrt{M^2-1} - (w \sin(\theta+\theta_c) + q_\infty \,.\, c_f \,.\, \cos\kappa)\sqrt{1+\frac{K}{M^2}\left(\frac{r}{r_0}\right)^2} \qquad \text{(C.4)}$$

$$T\frac{d\theta}{ds} = (p_l - p_u)\left(1+\frac{K}{M^2}\left(\frac{r}{r_0}\right)^2\right) - w \,.\, \cos(\theta+\theta_c)\sqrt{1+\frac{K}{M^2}\left(\frac{r}{r_0}\right)^2} \qquad \text{(C.5)}$$

in which κ = local cross-flow in the boundary layer.

If T is eliminated between equations (C.4) and (C.5), then

$$(p_l - p_u)\frac{K}{M^2}\left(\frac{r}{r_0}\right)^2 \sqrt{M^2-1} - (w \sin(\theta+\theta_c) + q_\infty\, c_f \cos\kappa)\sqrt{1+\frac{K}{M^2}\left(\frac{r}{r_0}\right)^2}$$

$$= \frac{dT}{ds}$$

$$= \frac{d}{ds}\left[\frac{ds}{d\theta}\left\{(p_l - p_u)\left(1+\frac{K}{M^2}\left(\frac{r}{r_0}\right)^2\right) - w\cos(\theta+\theta_c)\sqrt{1+\frac{K}{M^2}\left(\frac{r}{r_0}\right)^2}\right\}\right]$$

$$= \frac{dE}{d\theta} + E\frac{d\theta}{ds}\frac{d}{d\theta}\left(\frac{ds}{d\theta}\right),$$

$$E = \left\{ (p_l - p_u)\left(1 + \frac{K}{M^2}\left(\frac{r}{r_0}\right)^2\right) - w \cdot \cos(\theta + \theta_c)\sqrt{1 + \frac{K}{M^2}\left(\frac{r}{r_0}\right)^2} \right\}. \tag{C.6}$$

In the previous analysis (Appendix B) the term $w \sin(\theta + \theta_c)$ was neglected and for singly curved compression surfaces, the distribution of κ, the cross-flow in the boundary layer at the surface, cannot be calculated analytically until current work[39] to extend the method of Cooke and Jones[33] is completed; thus the present analysis is restricted to the caret sail in non-viscous flow and $w \cdot \sin(\theta + \theta_c)$ is neglected. Equation (C.6) can then be simplified to

$$(p_l - p_u)\frac{K}{M^2}\sqrt{M^2 - 1}\left(\frac{r}{r_0}\right)^2 d\theta - dE = E\, d\left(\frac{ds}{d\theta}\right)\Big/\left(\frac{ds}{d\theta}\right) \tag{C.7}$$

and integrated to yield

$$\log_e C\left(\frac{ds}{d\theta}\right) = \int \frac{(p_l - p_u)}{E}\frac{K}{M^2}\sqrt{M^2 - 1}\left(\frac{r}{r_0}\right)^2 d\theta - \log_e E = I'$$

i.e.

$$\frac{ds}{d\theta} = \frac{\exp I'}{C} = \frac{dx}{\cos\theta \cdot d\theta} = \frac{dy}{\sin\theta \cdot d\theta}.$$

The sail profile is therefore given by

$$\int dx = \int \frac{\exp I'}{C}\cos\theta \cdot d\theta, \int dy = \int \frac{\exp I'}{C}\sin\theta \cdot d\theta,$$

in which C can be found as follows:

$$C = (\exp I')\frac{d\theta}{ds} = \frac{E}{T}\exp I' = \text{constant}.$$

At some point on the sail where $s = s''$, $\theta = \theta''$, $T = T''$, $M = M''$,

$$C = \frac{1}{T''}\left\{ (p_l'' - p_u)\left(1 + \frac{K}{M''^2}\left(\frac{r''}{r_0}\right)^2\right) - w\cos(\theta'' + \theta_c)\sqrt{1 + \frac{K}{M''^2}\left(\frac{r''}{r_0}\right)^2} \right\} \exp\left([I']_{\Theta}^{\theta''}\right);$$

but at the leading edge of the sail, $\theta = \Theta, M = M_1, [I']_{\Theta}^{\Theta} = 0$,

therefore

$$C = \frac{p_{T1}}{T_{\text{l.e.}}}C' = \frac{p_{T1}}{T_{\text{l.e.}}}\left\{ \left(\left(1 + \frac{\gamma - 1}{2}M_1^2\right)^{-\frac{\gamma}{\gamma - 1}} - \frac{p_u}{p_{T1}} \right)\left(1 + \frac{K}{M_1^2}\left(\frac{r_1}{r_0}\right)^2\right) - \frac{w}{p_{T1}}\cos(\Theta + \theta_c)\sqrt{1 + \frac{K}{M_1^2}\left(\frac{r_1}{r_0}\right)^2} \right\}$$

in which C' is constant.

The sail profile is therefore given by

$$\frac{p_{T1}\,x}{T_{\text{l.e.}}} = \int_{\Theta}^{\theta} \frac{1}{C'} \exp\left([I']_{\Theta}^{\bar{\theta}}\right) \cos\bar{\theta}\,.\,d\bar{\theta}\,,\quad \frac{p_{T1}\,y}{T_{\text{l.e.}}} = \int_{\Theta}^{\theta} \frac{1}{C'} \exp\left([I']_{\Theta}^{\bar{\theta}}\right) \sin\bar{\theta}\,.\,d\bar{\theta}\,. \tag{C.8}$$

TABLE 1

Values of Parameters in Figs. 6 to 9.

M_∞, M_{comp}	M_N, η_{KE}, Θ and M_1	p_u/p_∞	w/p_∞	$\frac{p_u + w\cos(\Theta+\theta_c)}{p_{T1}}$	$p_{T1}\, x/T$	Figure number
$M_\infty = 10$ $M_{comp} = 3{\cdot}5$	$M_N = 1$ $\eta_{KE} = 1$	0	0 0·2 0·4	0 0·0000047(1) 0·0000094(2)	3500 3875 4393	6(a)
	$\Theta = 0°$ $M_1 = 10$	0·5	0 0·2 0·4	0·000011(8) 0·000016(5) 0·000021(2)	4743 5799 8410	6(b)
	$M_N = 1{\cdot}4$ $\eta_{KE} = 0{\cdot}9994$	0·5	0 0·2 0·4	0·000012(3) 0·000017(2) 0·000022(1)	1991 2110 2252	7(a)
	$\Theta = 3{\cdot}264°$ $M_1 = 8{\cdot}8705$	1·0	0 0·2 0·4	0·000024(6) 0·000029(5) 0·000034(4)	2336 2533 2789	7(b)
	$M_N = 2{\cdot}6$ $\eta_{KE} = 0{\cdot}9876$	0·5	0 0·2 0·4	0·000025(6) 0·000035(7) 0·000045(7)	304·2 308·2 312·4	7(c)
	$\Theta = 10{\cdot}606°$ $M_1 = 6{\cdot}4738$	1·0	0 0·2 0·4	0·000051(2) 0·000061(3) 0·000071(3)	314·8 319·3 323·9	7(d)
$M_\infty = 7$ $M_{comp} = 2{\cdot}5$	$M_N = 1{\cdot}2$ $\eta_{KE} = 0{\cdot}9998$	0·5	0 0·2 0·4	0·00012(2) 0·00017(0) 0·00021(9)	391·5 431·2 485·2	8(a)
	$\Theta = 2{\cdot}481°$ $M_1 = 6{\cdot}5477$	1·0	0 0·2 0·4	0·00024(3) 0·00029(2) 0·00034(0)	521·8 627·8 871·6	8(b)
	$M_N = 2{\cdot}0$ $\eta_{KE} = 0{\cdot}9900$	0·5	0 0·2 0·4	0·00016(7) 0·00023(3) 0·00029(9)	91·07 93·47 96·04	8(c)
	$\Theta = 10{\cdot}222°$ $M_1 = 5{\cdot}1962$	1·0	0 0·2 0·4	0·00033(5) 0·00040(1) 0·00046(7)	97·61 100·5 103·6	8(d)

$M_\infty = 4$	$M_N = 1{\cdot}2$	0·5	0	0·0033(2)	24·31	9(a)
			0·2	0·00464	26·79	
	$\eta_{KE} = 0{\cdot}9993$		0·4	0·00596	30·16	
	$\Theta = 4{\cdot}265°$	1·0	0	0·00663	32·56	9(b)
			0·2	0·0079(6)	39·22	
	$M_1 = 3{\cdot}6901$		0·4	0·00928	54·49	
$M_{comp} = 1{\cdot}5$	$M_N = 1{\cdot}6$	0·5	0	0·0036(8)	11·16	9(c)
			0·2	0·0051(2)	11·65	
	$\eta_{KE} = 0{\cdot}9900$		0·4	0·0065(6)	12·20	
	$\Theta = 11{\cdot}455°$	1·0	0	0·0073(6)	12·58	9(d)
			0·2	0·008(80)	13·26	
	$M_1 = 3{\cdot}1828$		0·4	0·0102(4)	14·05	

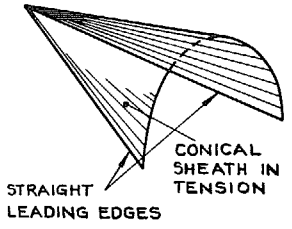

(a) N.A.S.A. PARAWING

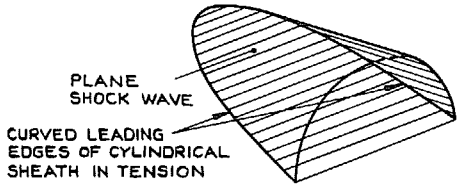

(b) PLANE SHOCK PARAWING
(SINGLE SHOCK, n=1)

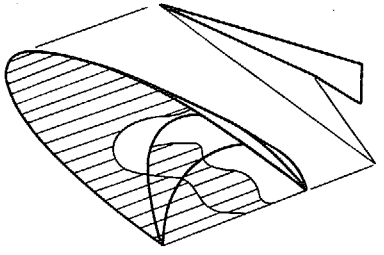

(c) PLANE SHOCK PARAWING
(TWIN SHOCKS, n = 2)

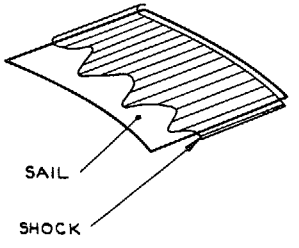

(d) TWO-DIMENSIONAL SAIL
IN NEWTONIAN FLOW

FIG. 1 a to d. Flexible surfaces in supersonic flows.

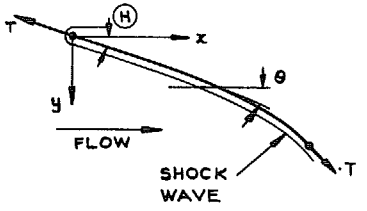

(a) BOYD'S MODEL (SEE REF. 20)

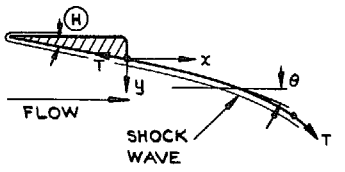

(b) ALTERNATIVE MODEL

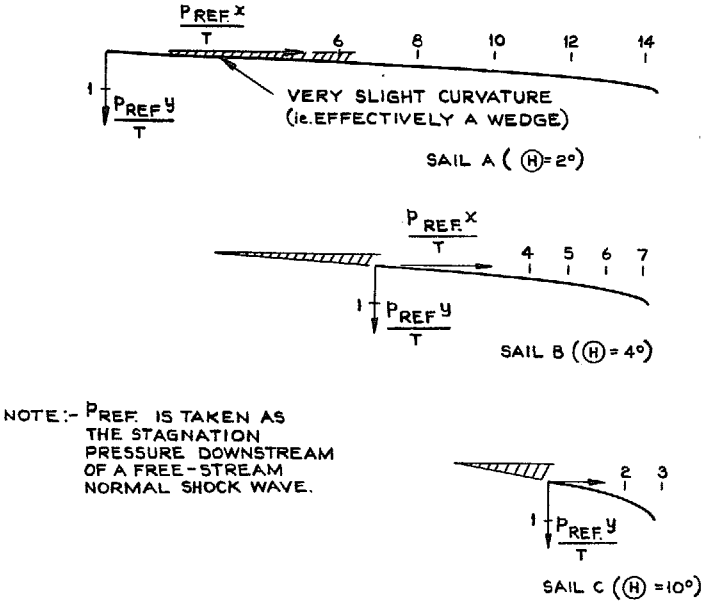

(c) TYPICAL SAIL PROFILES

FIG. 2 a to c. Two-dimensional sails in supersonic flow (calculated as by Boyd[20] using Newton-Busemann pressure law).

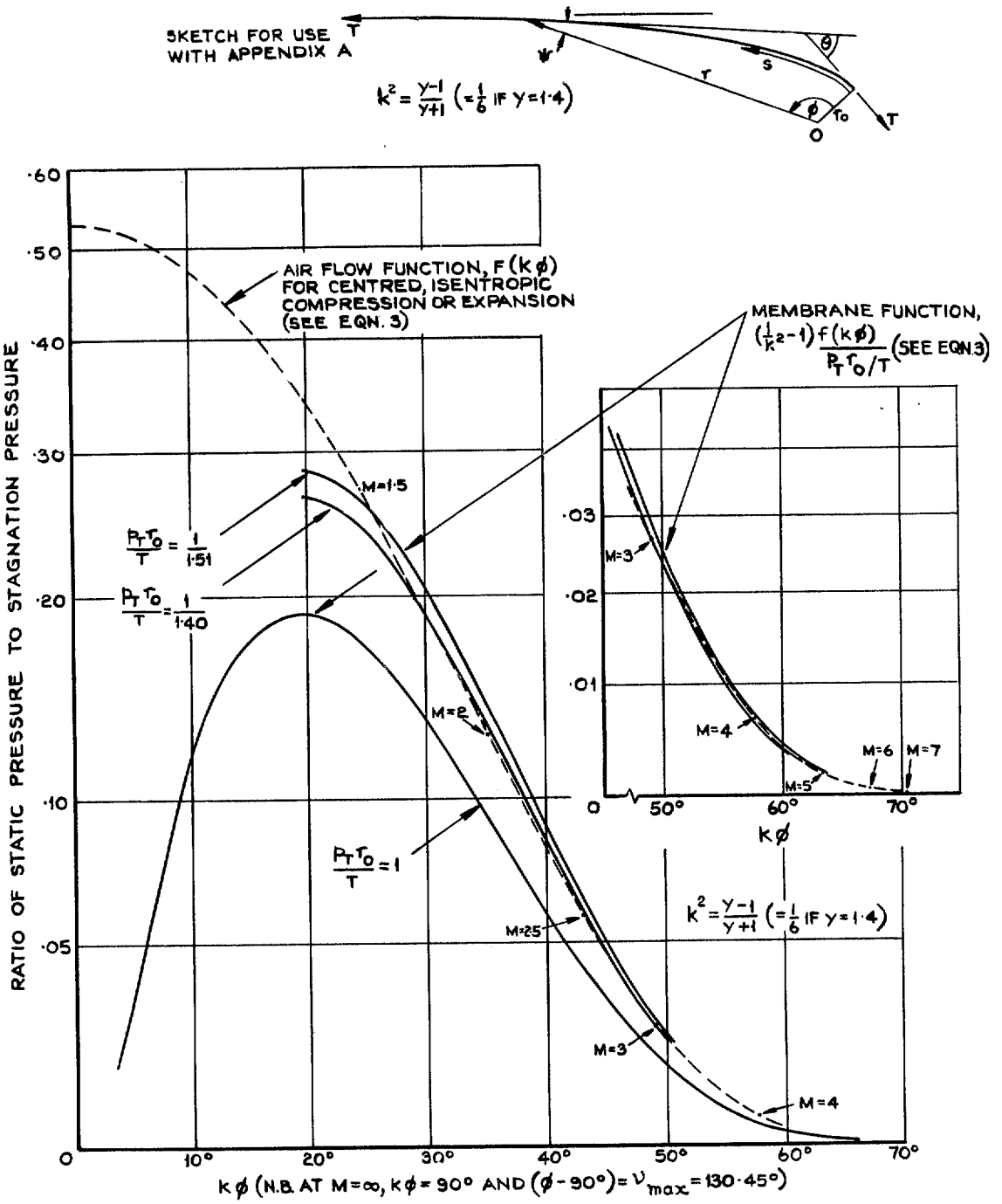

FIG. 3. Variation with local Mach number of aerodynamic and geometric properties for a sail producing centred compression.

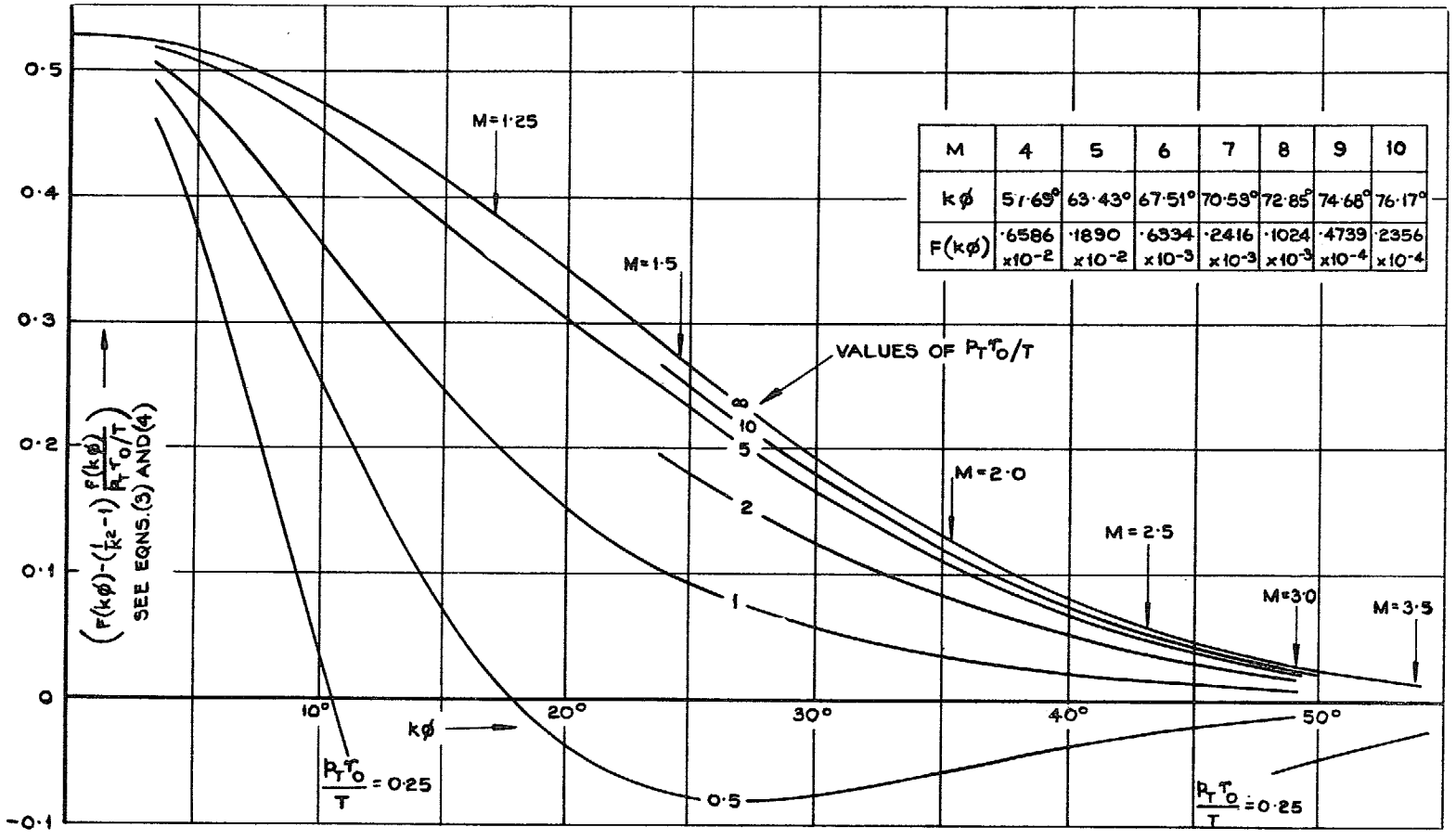

FIG. 4. Variation of $\left[F(k\phi)-\left(\frac{1}{k^2}-1\right)\frac{f(k\phi)}{p_T r_0/T} \right]$ with $p_T r_0/T$ and $k\phi$.

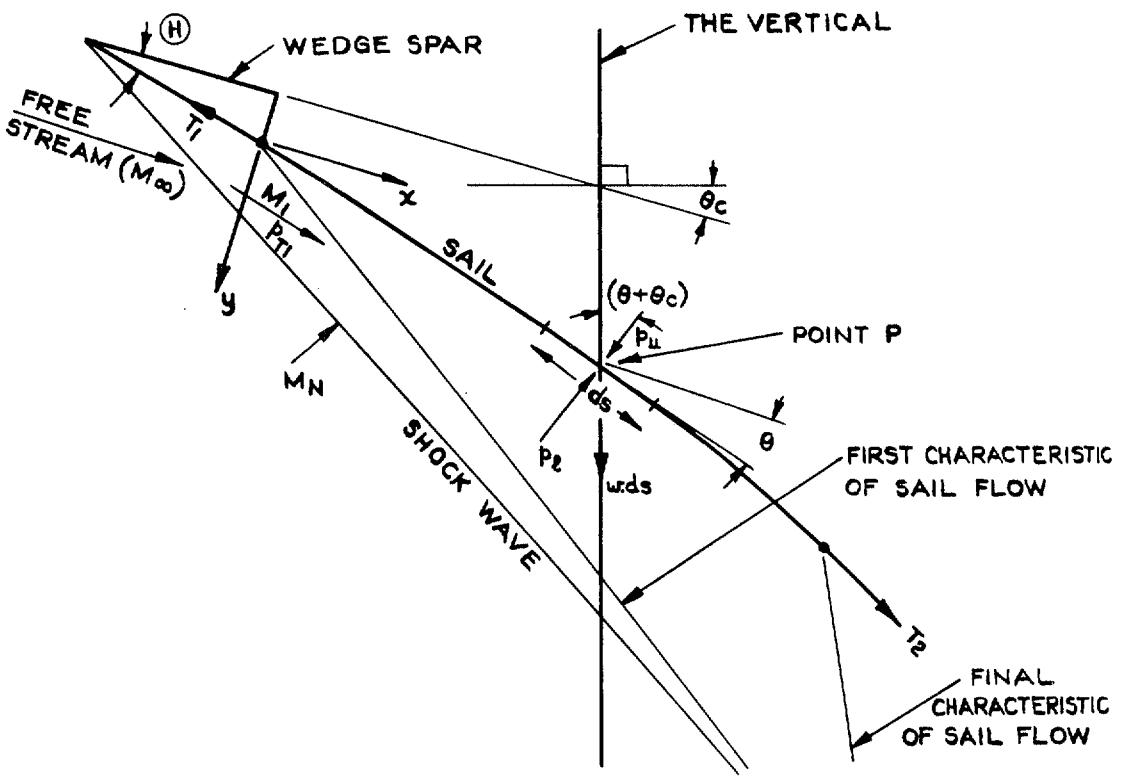

(a) SAIL MODEL ANALYSED

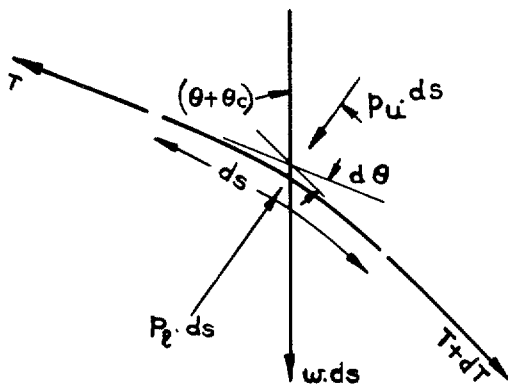

(b) SAIL ELEMENT OF UNIT WIDTH, AND LENGTH, ds.

FIG. 5 a & b. Features of model analysed : the sail with finite weight and upper-surface pressure.

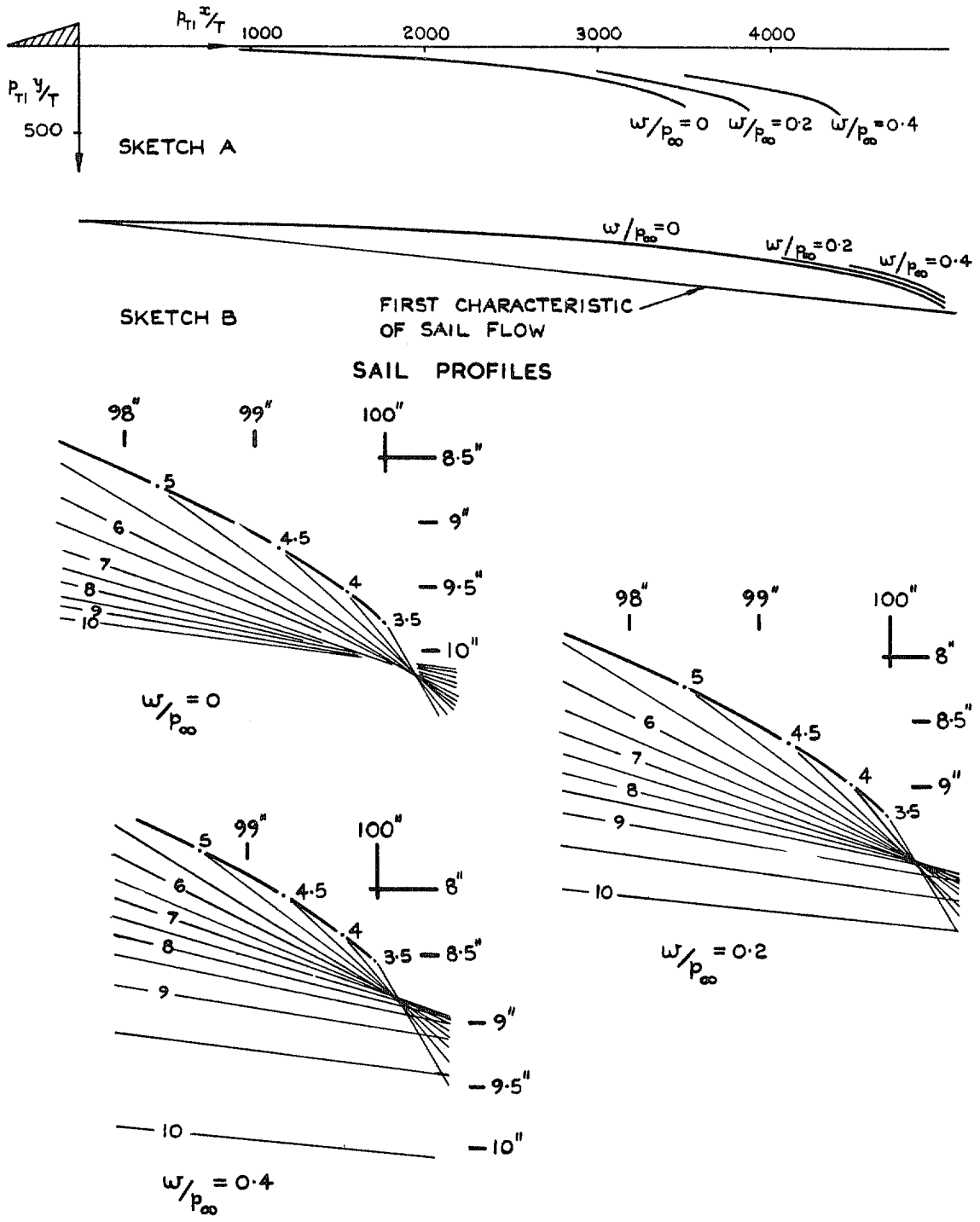

(a) $M_\infty = 10$, $pu/p_\infty = 0$

FIG. 6a. Two-dimensional, isentropic sail (i.e. $M_N = 1$), as influenced by weight and upper surface pressure.

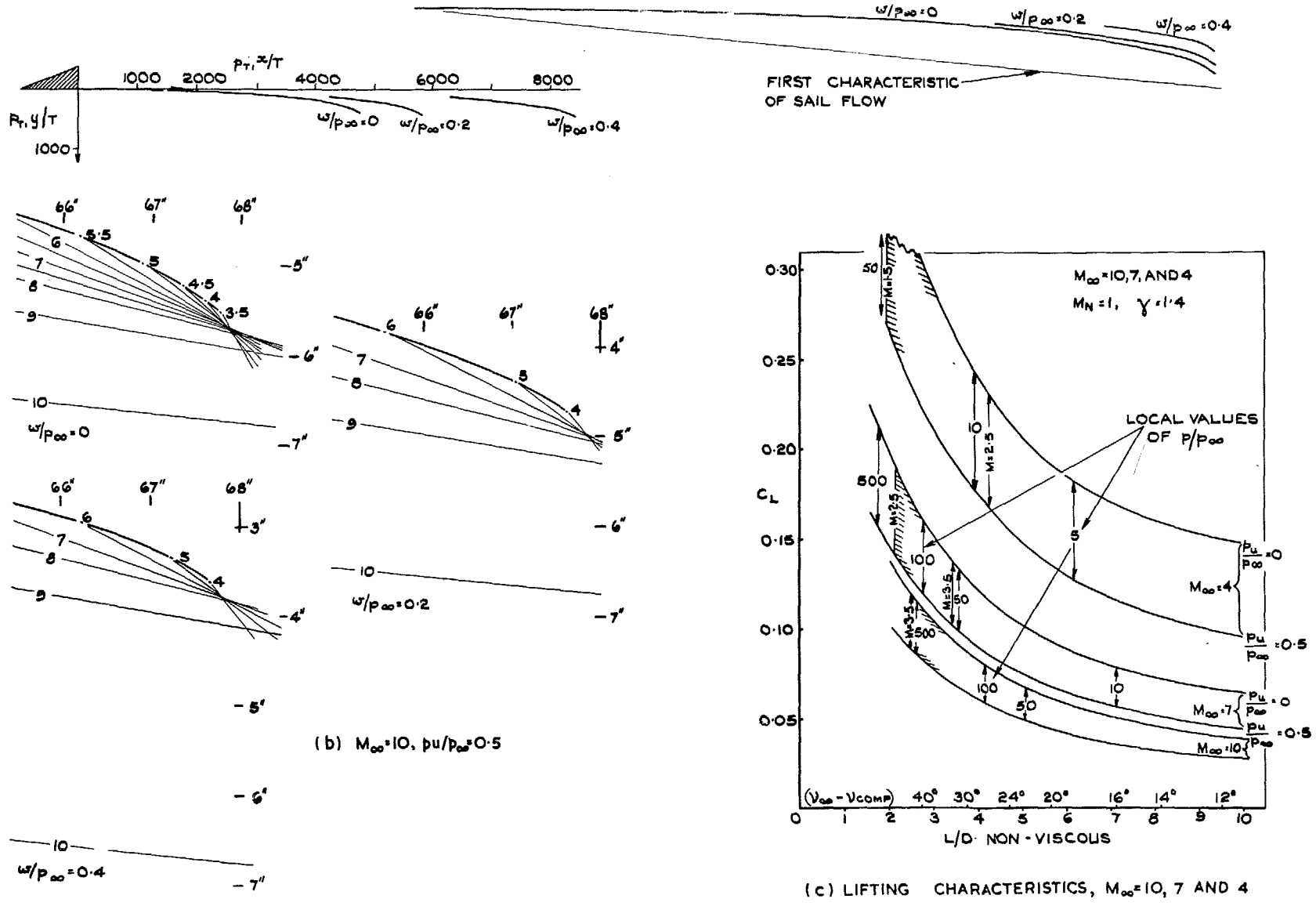

FIG. 6 b & c. Two-dimensional isentropic sail (i.e. $M_N = 1$), as influenced by weight and upper-surface pressure.

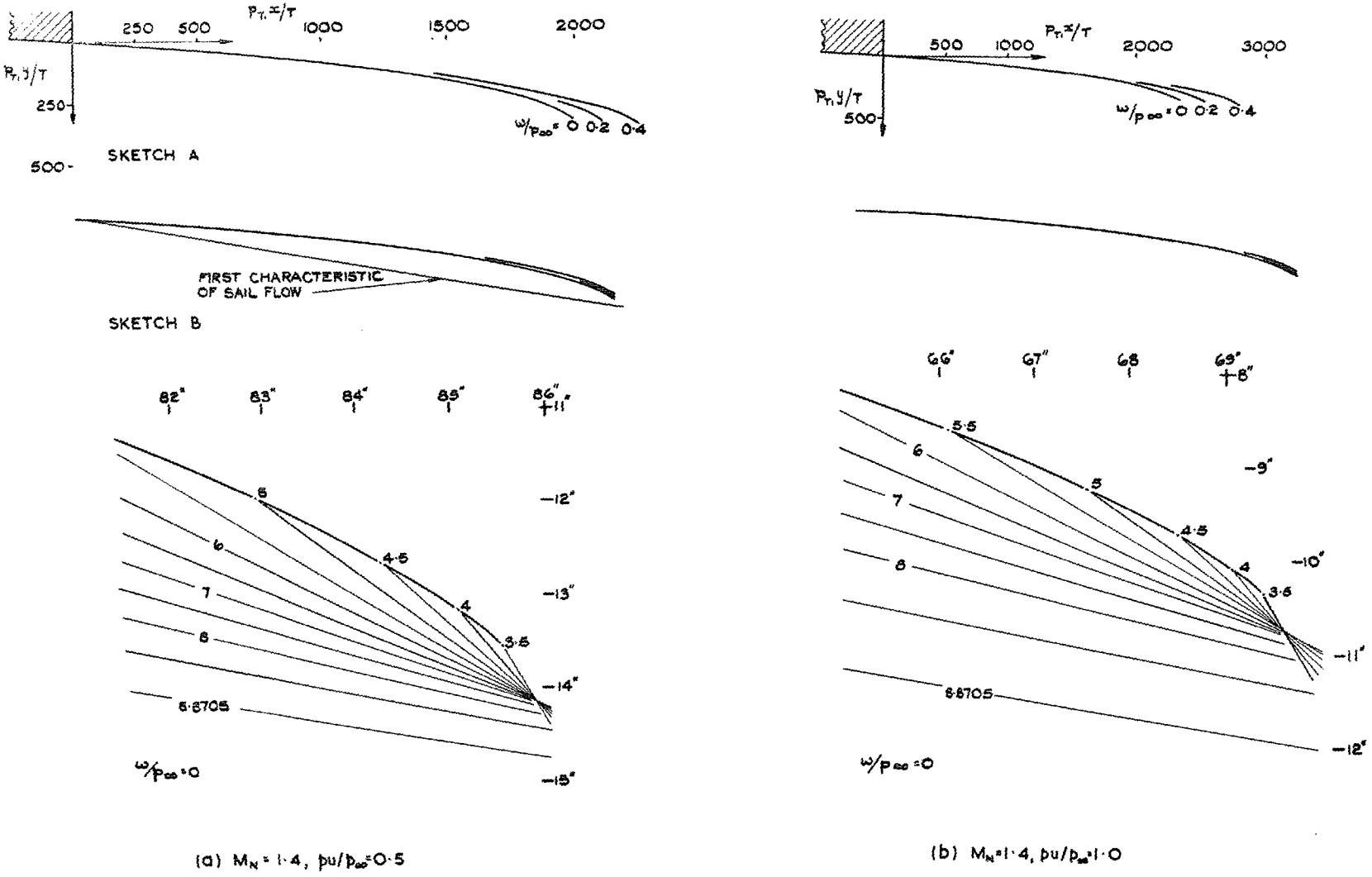

FIG. 7 a & b. Two-dimensional, wedge-spar-plus-sail at $M_\infty = 10$.

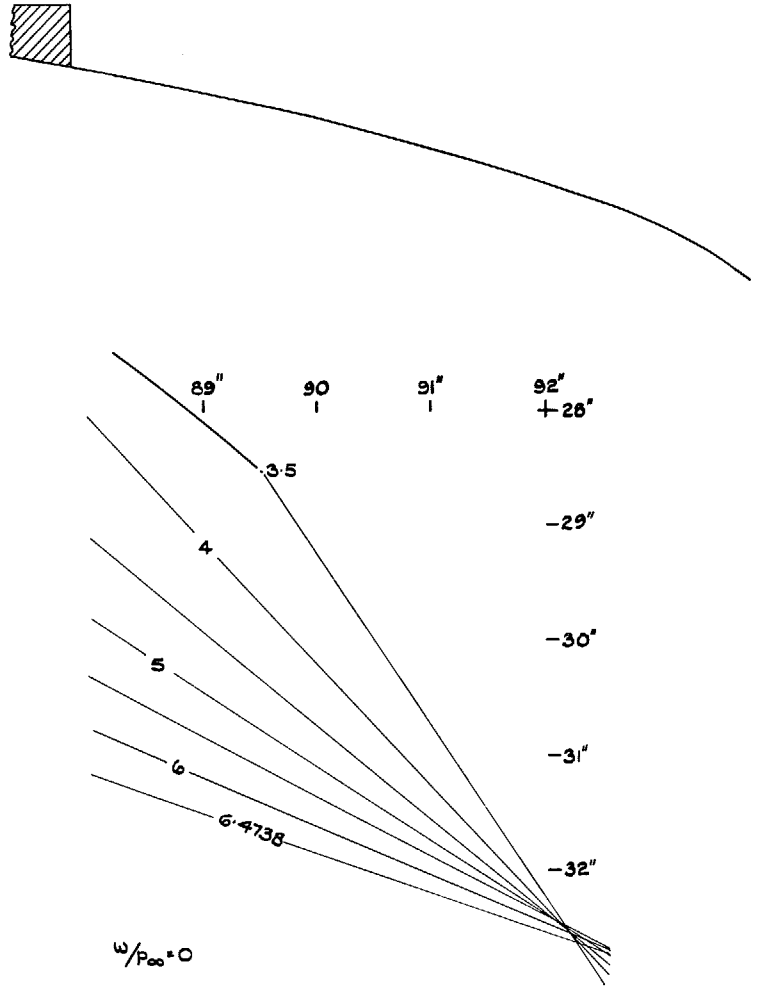

(c) $M_N = 2{\cdot}6$, $p_u/p_\infty = 0{\cdot}5$

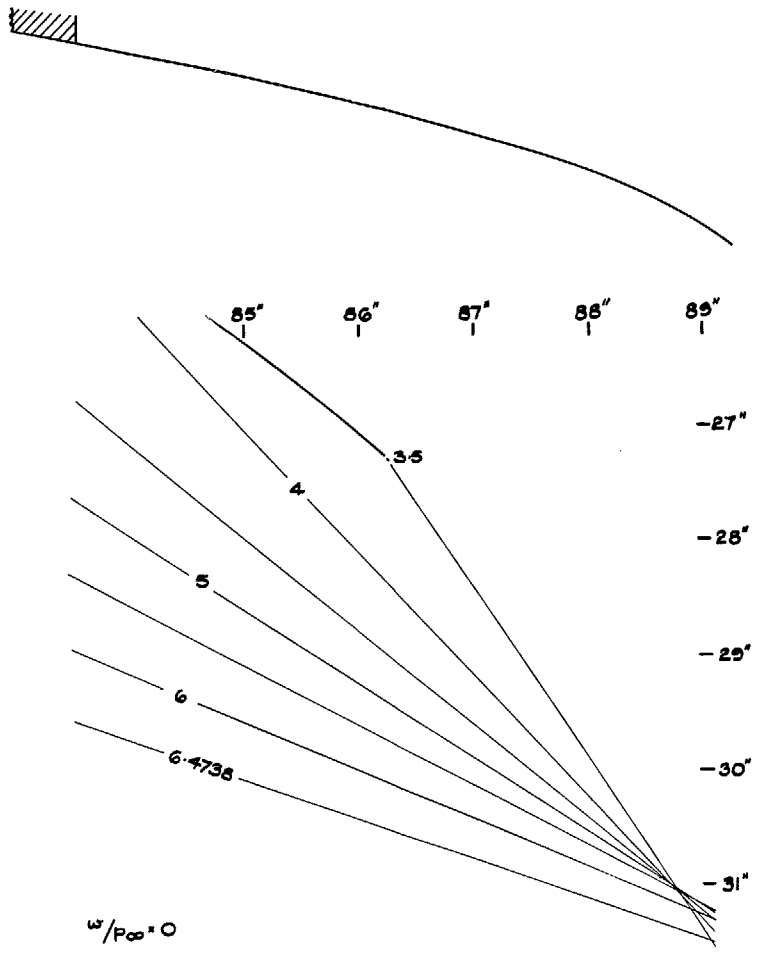

(d) $M_N = 2{\cdot}6$, $p_u/p_\infty = 1{\cdot}0$

FIG. 7 c & d. Two-dimensional, wedge-spar-plus-sail at $M_\infty = 10$.

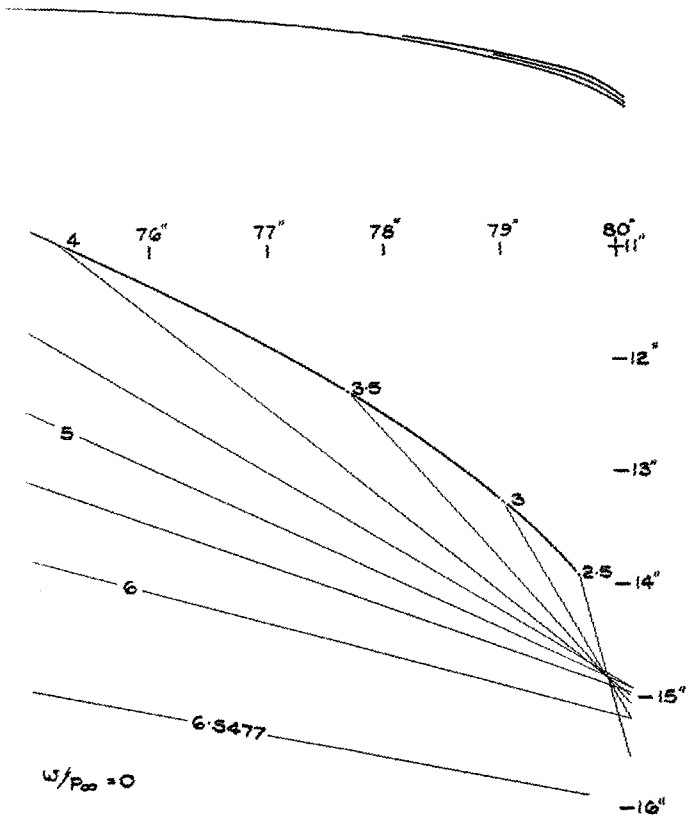

(a) $M_N = 1{\cdot}2$, $p_u/p_\infty = 0{\cdot}5$

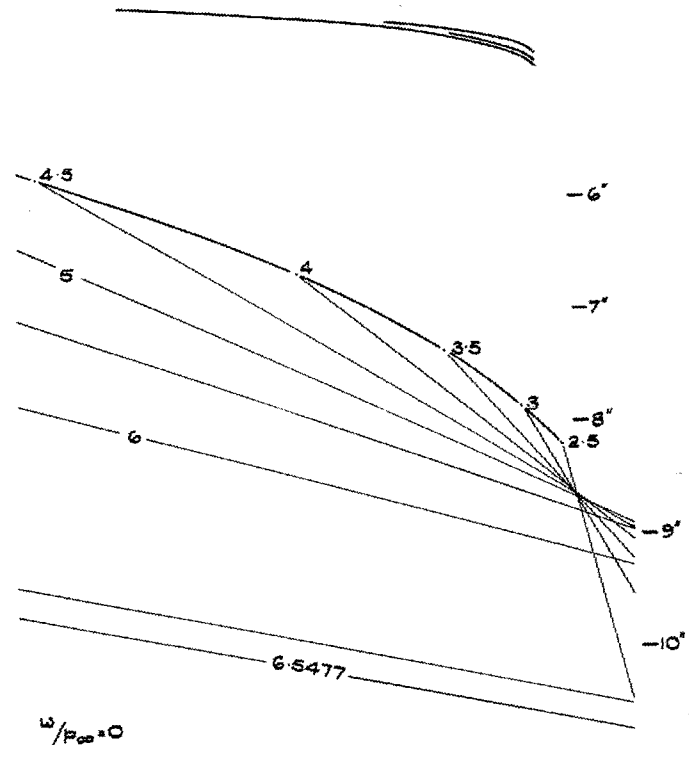

(b) $M_N = 1{\cdot}2$, $p_u/p_\infty = 1{\cdot}0$

FIG. 8 a & b. Two-dimensional, wedge-spar-plus-sail at $M_\infty = 7$.

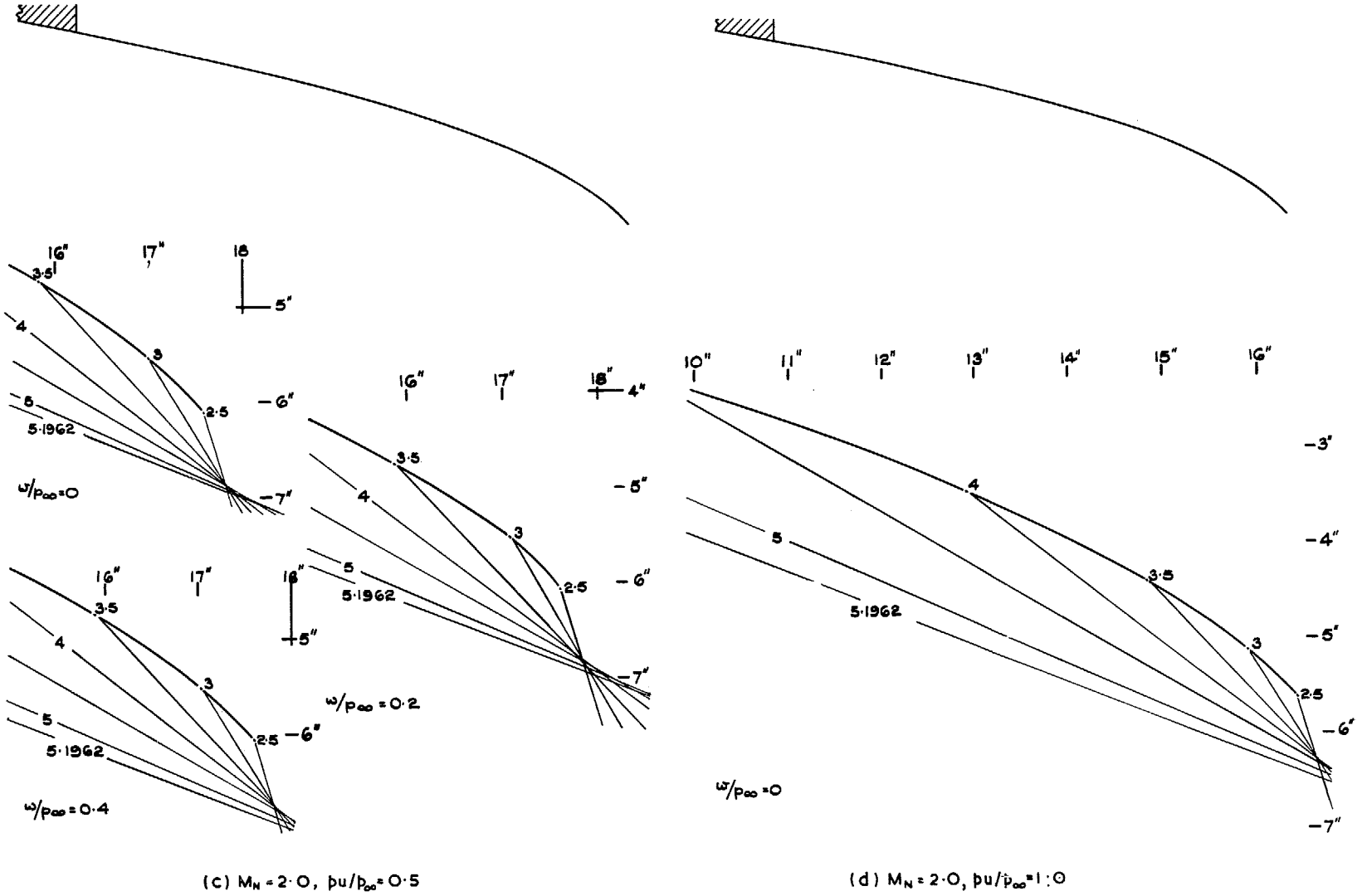

FIG. 8 c & d. Two-dimensional, wedge-spar-plus-sail at $M_\infty = 7$.

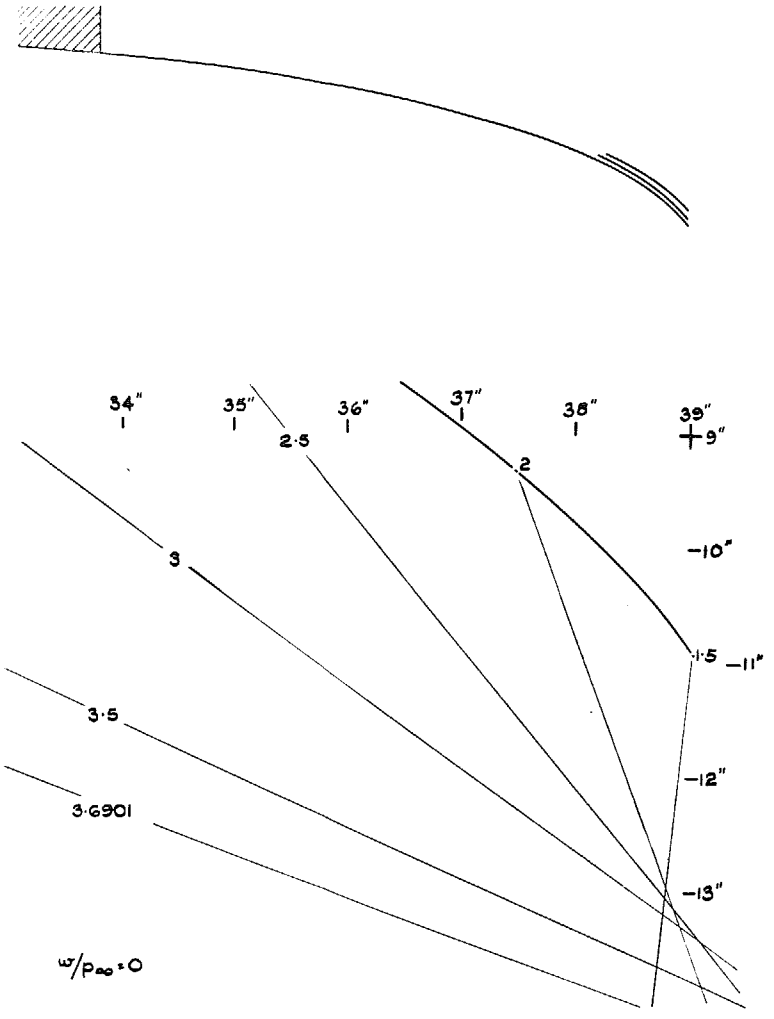

(a) $M_N = 1{\cdot}2$, $p_u/p_\infty = 0{\cdot}5$

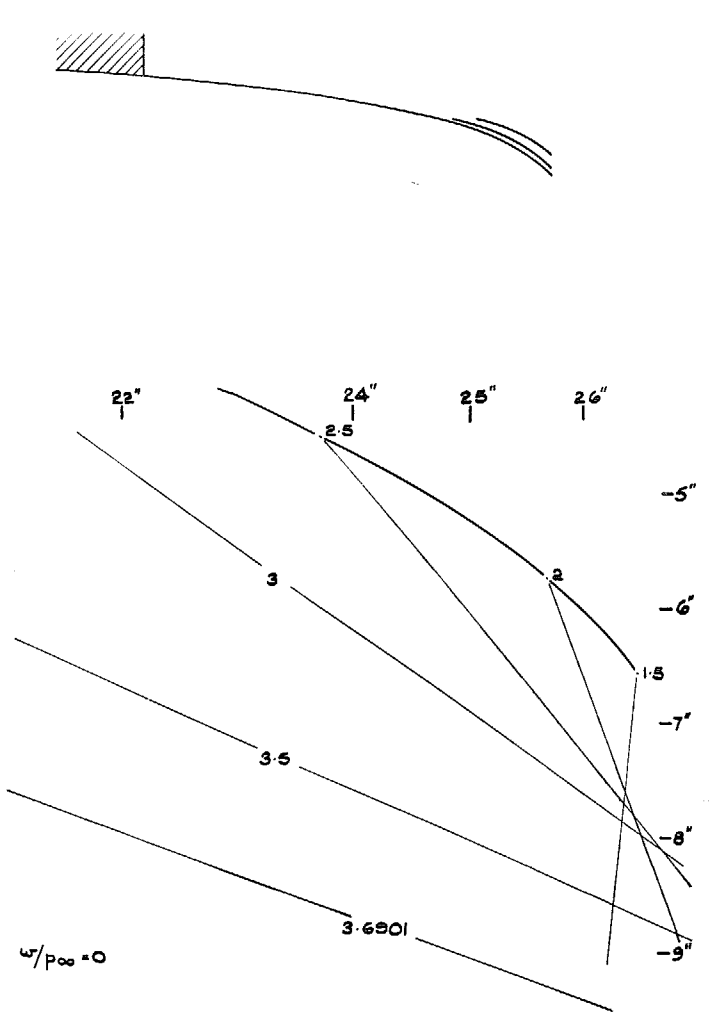

(b) $M_N = 1{\cdot}2$, $p_u/p_\infty = 1{\cdot}0$

FIG. 9 a & b. Two-dimensional, wedge-spar-plus-sail at $M_\infty = 4$.

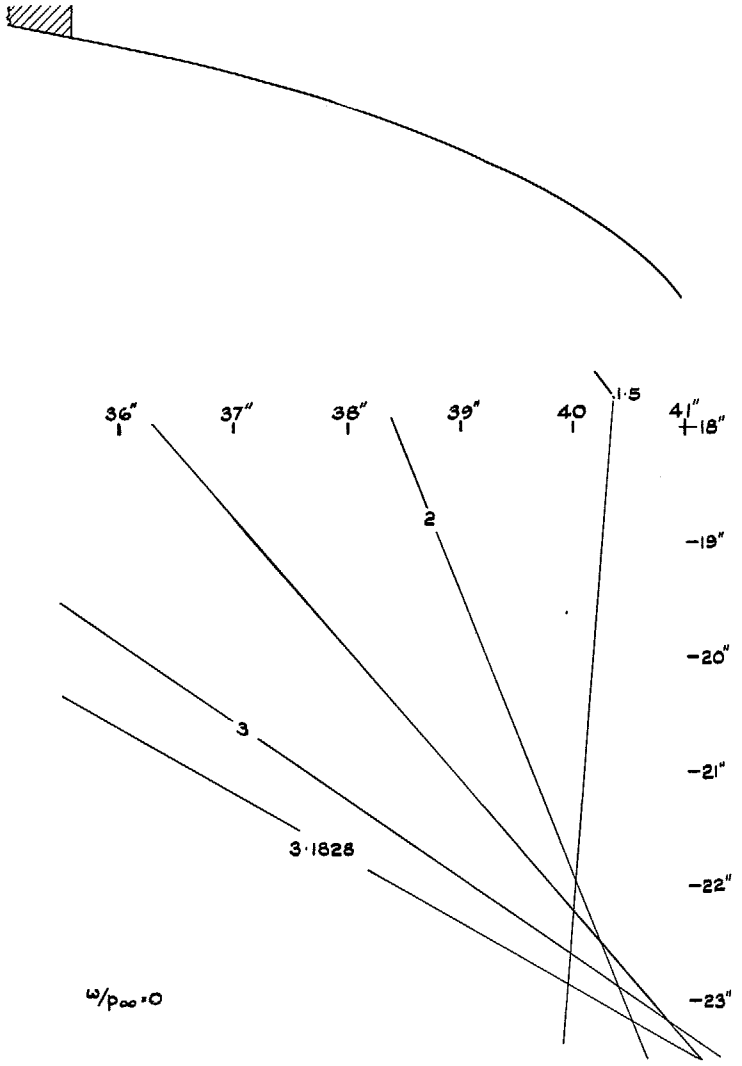

(c) $M_N = 1{\cdot}6$, $pu/p_\infty = 0{\cdot}5$

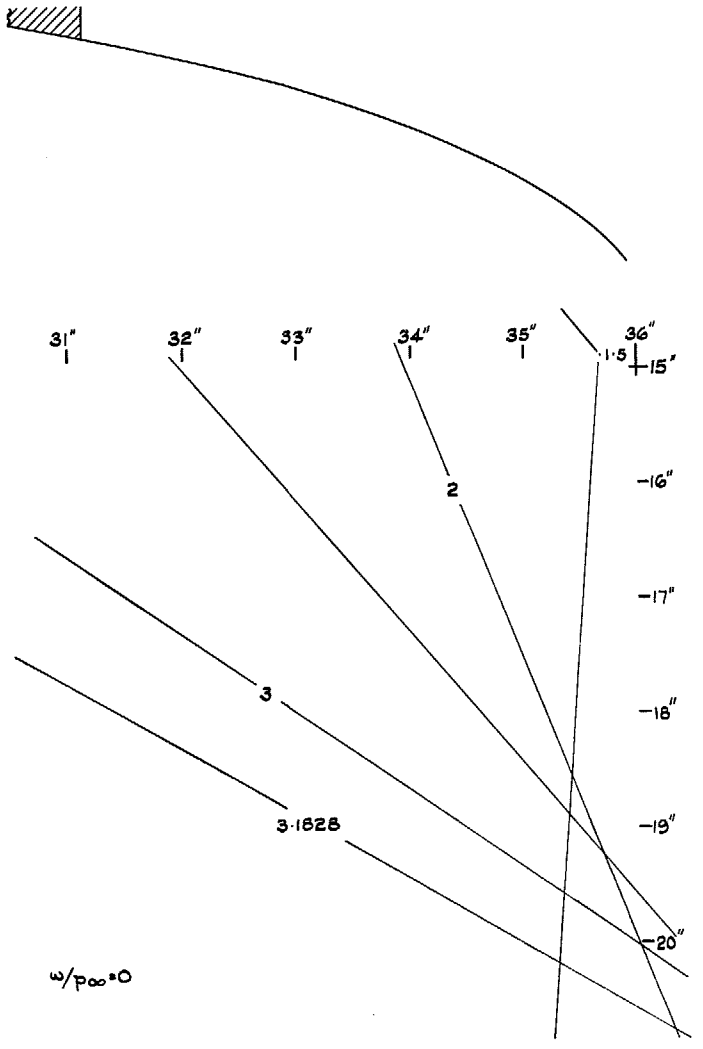

(c) $M_N = 1{\cdot}6$, $pu/p_\infty = 1{\cdot}0$

FIG. 9 c & d. Two-dimensional, wedge-spar-plus-sail at $M_\infty = 4$.

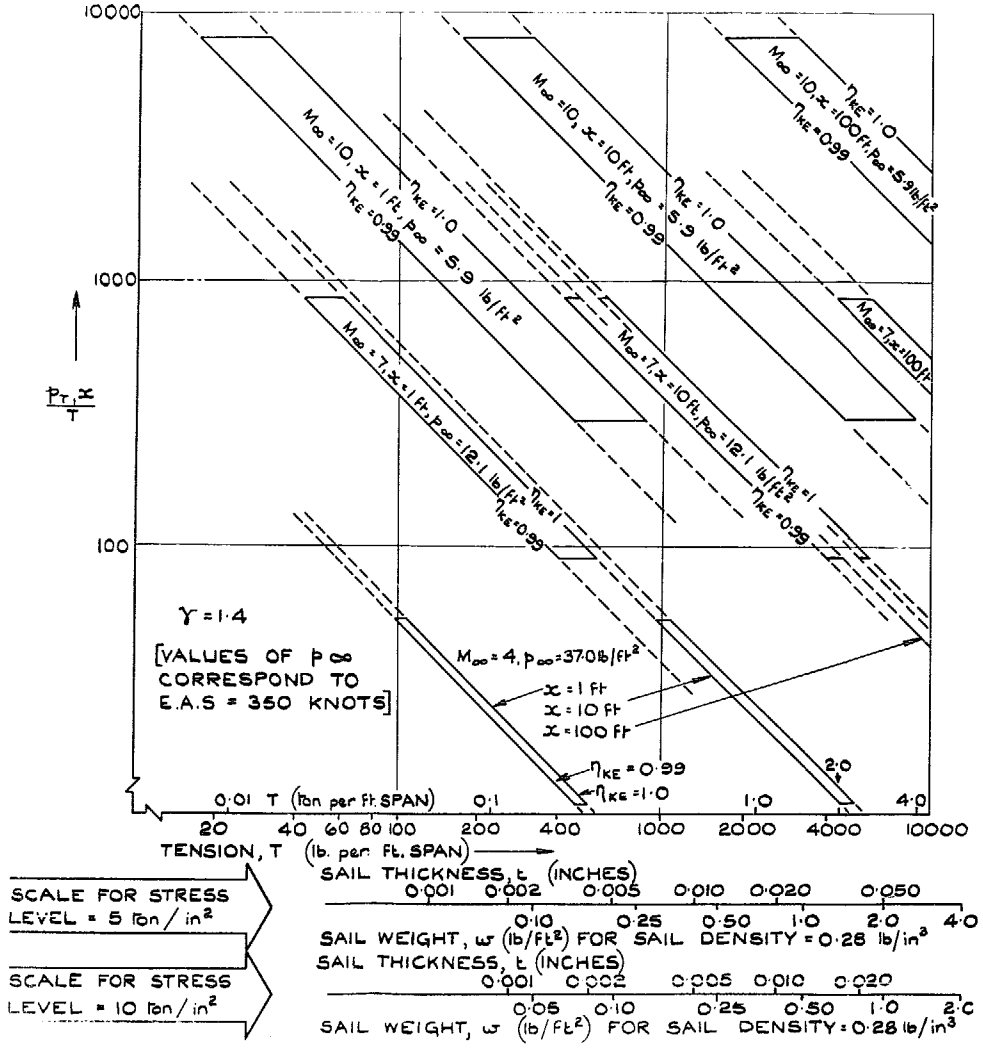

EAS (KNOTS)	250	300	350	400	450
p_∞ (lb/ft²)	3·023	4·354	5·926	7·740	9·796
APPROX. ALTITUDE (FT)	150,000	141,000	133,000	126,000	120,000

$M_\infty = 10, \gamma = 1.4$

EAS (KNOTS)	250	300	350	400	450
p_∞ (lb/ft²)	6·170	8·885	12·09	15·80	19·99
APPROX. ALTITUDE (FT)	132,000	123,000	115,000	109,000	104,000

$M_\infty = 7, \gamma = 1.4$

EAS (KNOTS)	250	300	350	400	450
p_∞ (lb/ft²)	18·90	27·21	37·04	48·38	61·23
APPROX ALTITUDE (FT)	105,000	97,000	90,000	84,000	79,000

$M_\infty = 4, \gamma = 1.4$

FIG. 10. Variation with operating conditions of sail tension, stress, thickness and weight.

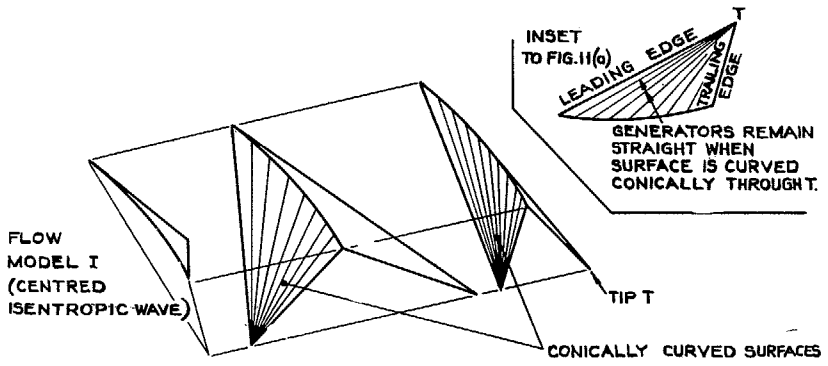

(a) CONICALLY CURVED CARET SURFACES

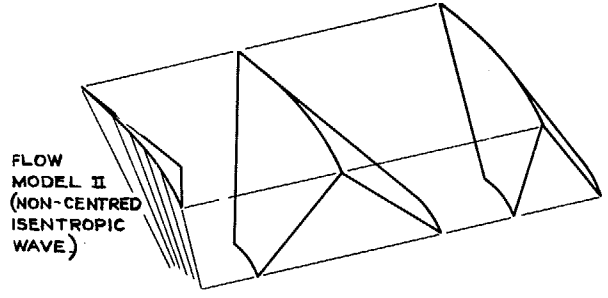

(b) NON-CONICAL, SINGLY CURVED CARET SURFACES

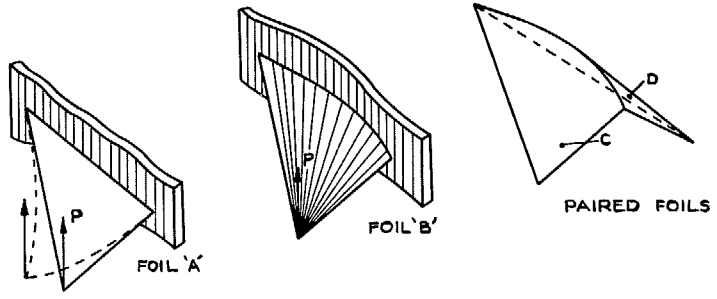

(c) STIFFNESS ACQUIRED BY A FOIL DUE TO CURVATURE

FIG. 11 a to c. Surfaces to contain two-dimensional isentropic waves.

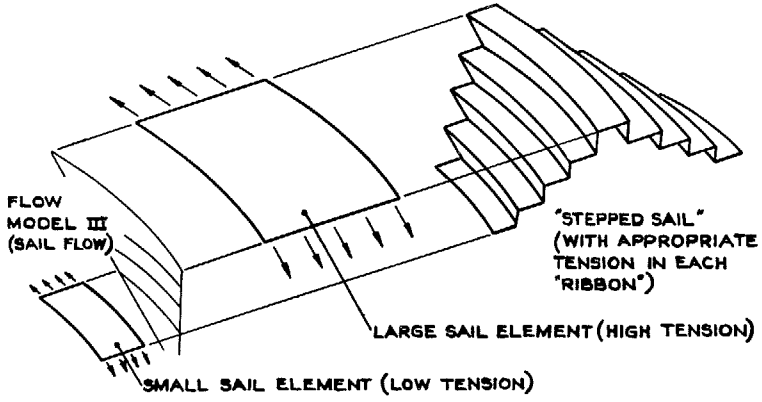

(a) TOP REAR VIEW OF TWO-DIMENSIONAL SAILS

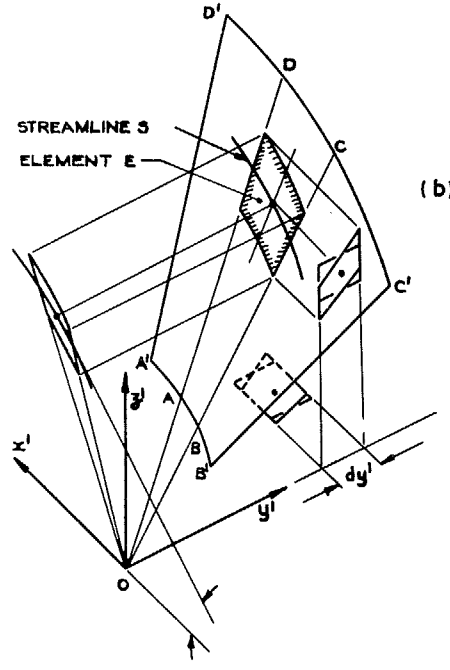

(b) GEOMETRY OF CARET SAIL

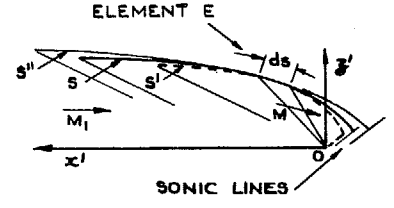

(c) POSSIBLE STREAMLINES THROUGH ELEMENT E

Fig. 12 a to c. Aerodynamic and geometric features of a caret sail.

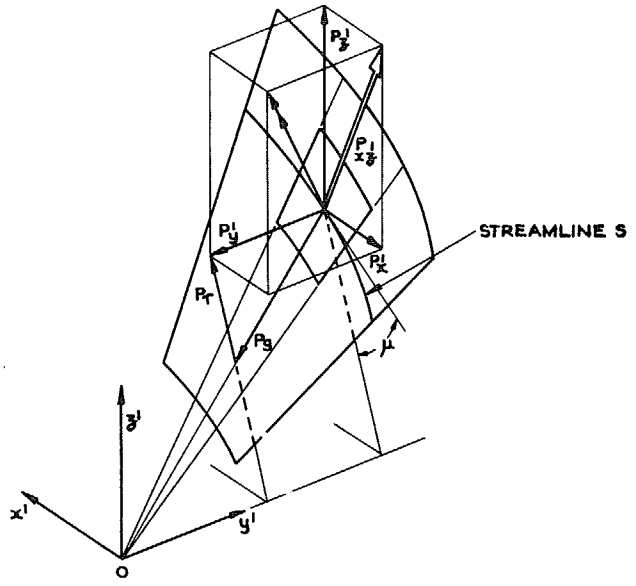

(a) COMPONENTS OF THE PRESSURE FORCE ON ELEMENT.E.

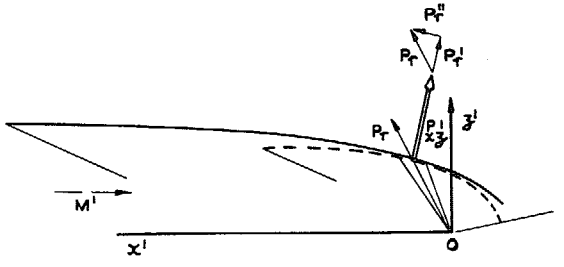

(b) COMPONENTS PARALLEL TO THE PLANE x'o z'

FIG. 13 a & b. Forces acting on a caret sail.

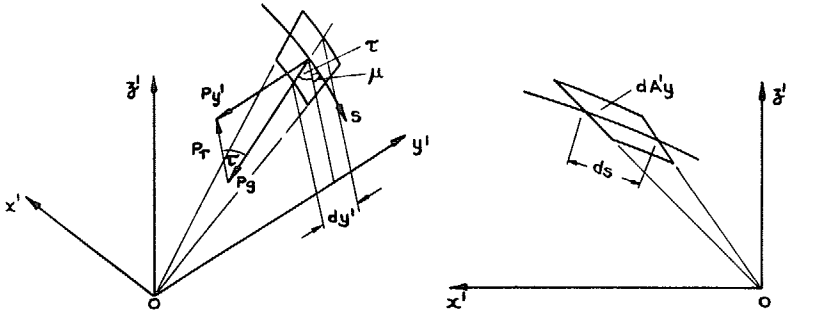

(c) LATERAL COMPONENTS OF AREA AND PRESSURE FORCE

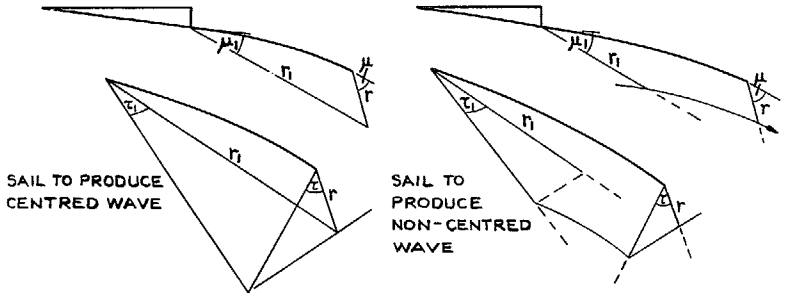

(d) GEOMETRY OF SINGLY CURVED SAILS

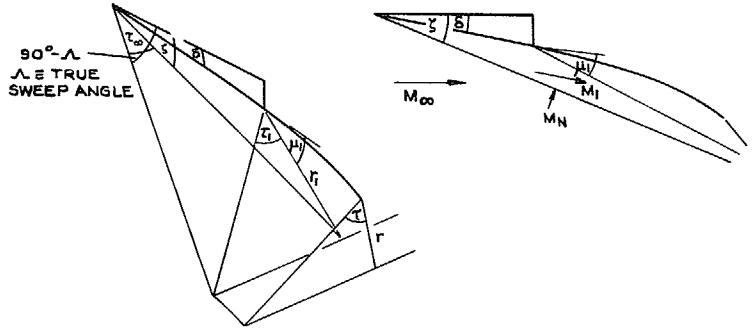

(e) GEOMETRY OF WEDGE-SPAR-PLUS-SAIL

FIG. 13 c to e. Forces acting on a caret sail.

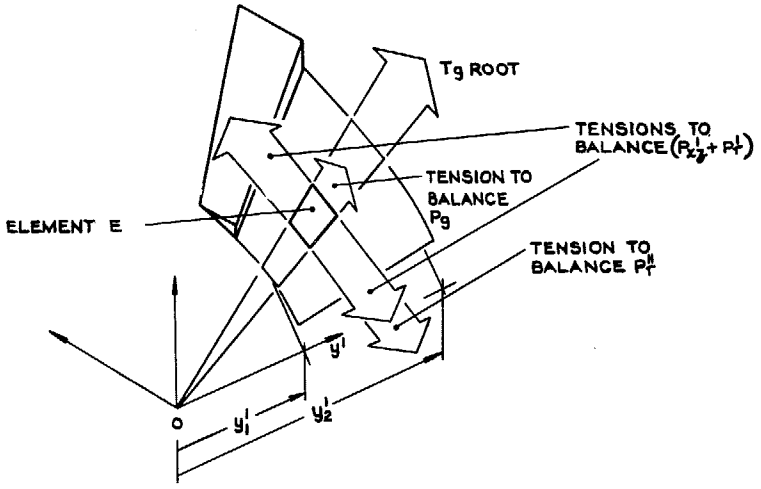

(f) TENSIONS TO BALANCE PRESSURE FORCE ON ELEMENT E

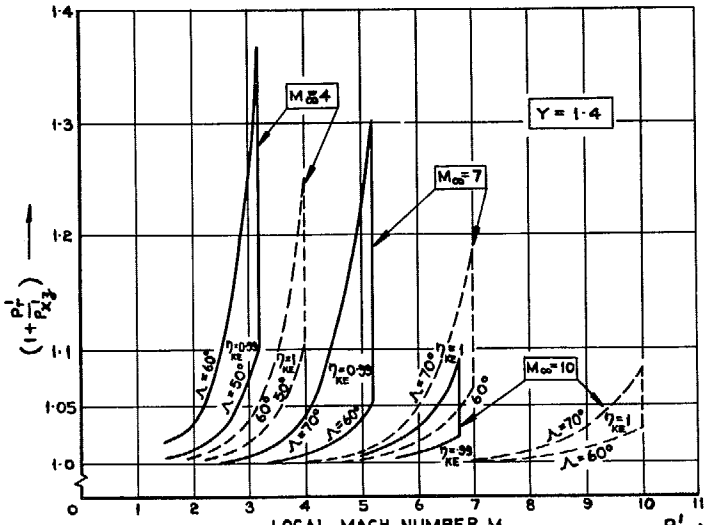

(g) VARIATION OF ANHEDRAL CORRECTION FACTOR $\left(1 + \frac{P_f^I}{P_{xy}^I}\right)$ WITH LOCAL MACH NUMBER

FIG. 13 f to g. Forces acting on a caret sail.

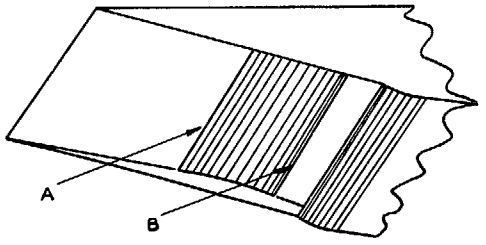

(a) WEDGE INTAKE

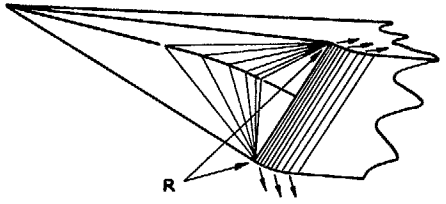

(b) CARET INTAKE

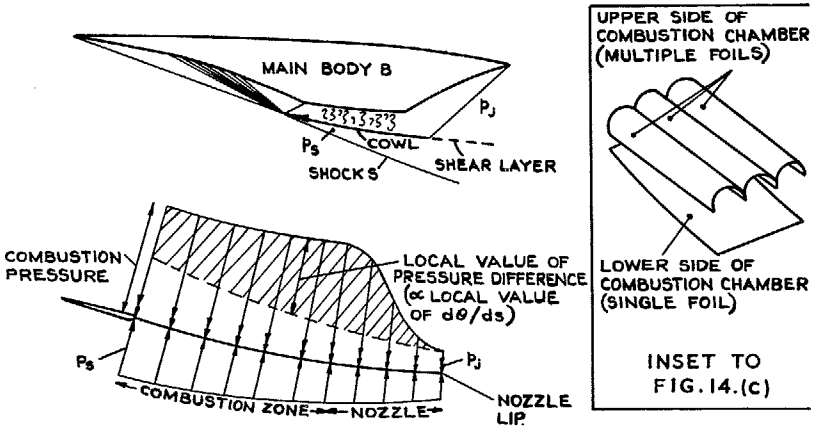

(c) FLEXIBLE COWL

FIG. 14 a to c. Intakes and cowls.

Printed in Wales for Her Majesty's Stationery Office by Allens Printers (Wales) Limited
Dd. 146916 K.5.

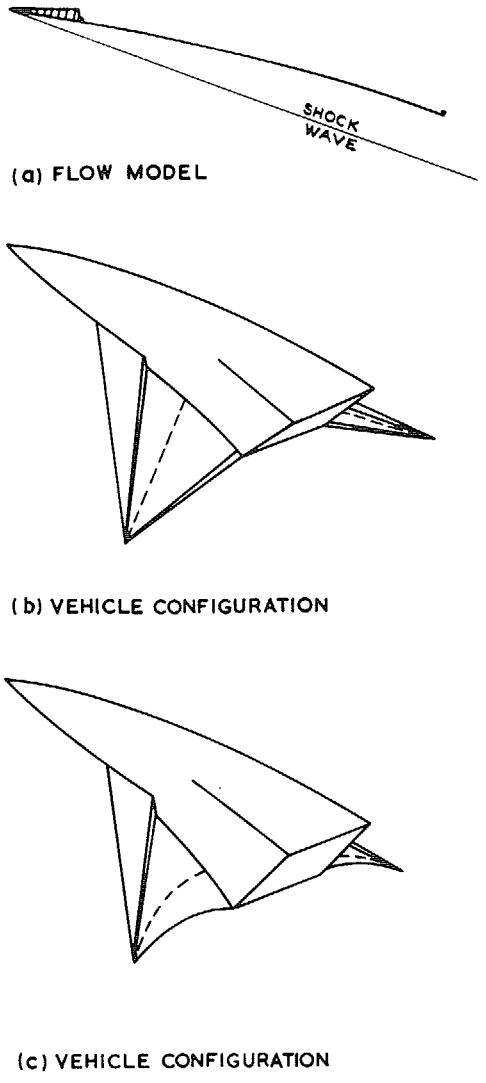

FIG. 15 a to c. Simple lifting system.

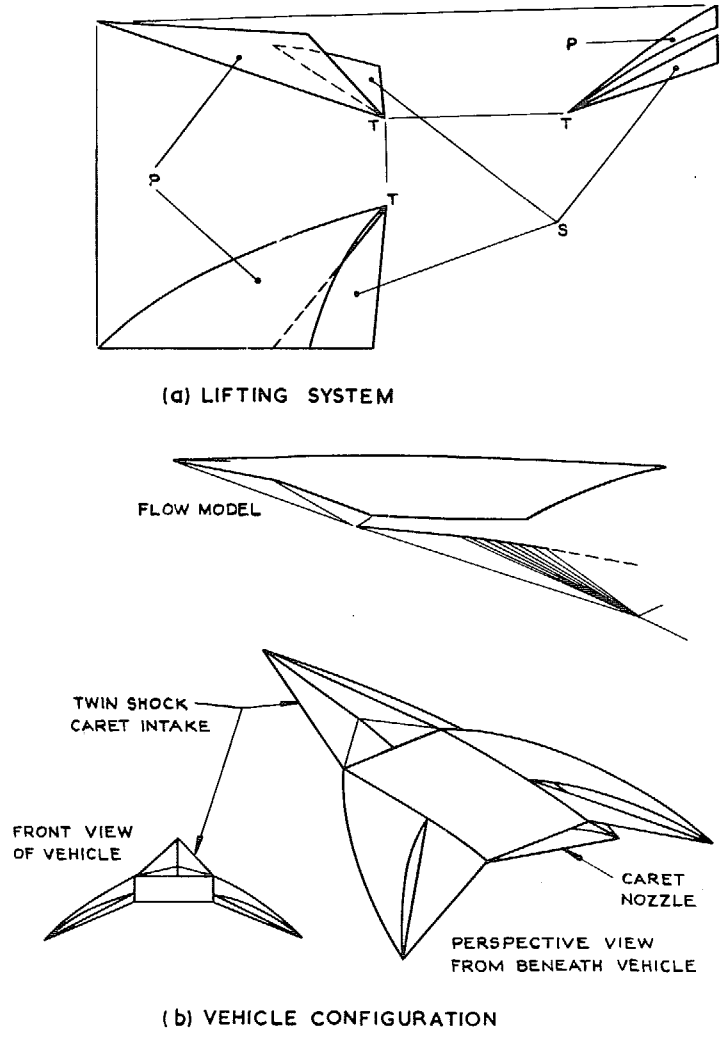

FIG. 16 a & b. Composite lifting system.

Published by
HER MAJESTY'S STATIONERY OFFICE

To be purchased from
49 High Holborn, London WC1
13a Castle Street, Edinburgh EH2 3AR
109 St Mary Street, Cardiff CF1 1JW
Brazennose Street, Manchester M60 8AS
50 Fairfax Street, Bristol BS1 3DE
258 Broad Street, Birmingham 1
7 Linenhall Street, Belfast BT2 8AY
or through any bookseller

SBN 11 470324 8